INTRAUTERINE FETAL GROWTH RESTRICTION AND SEXUALLY DIMORPHIC PROGRAMMING OF ADIPOCYTES

By

John Blomberg

A Thesis Presented to the Faculty of the

SCHOOL OF ANIMAL AND COMPARATIVE BIOMEDICAL SCIENCES

In Partial Fulfillment of the Requirements

For the Degree of

MASTER OF SCIENCE

In the Graduate College

THE UNIVERSITY OF ARIZONA

2021

THE UNIVERSITY OF ARIZONA
GRADUATE COLLEGE

As members of the Master's Committee, we certify that we have read the thesis prepared by: Jack Blomberg John Blomberg
titled: Intrauterine Growth Restriction and Sexually Dimorphic Programming of Adipocytes

and recommend that it be accepted as fulfilling the thesis requirement for the Master's Degree.

Ravi Goyal — Date: Jul 26, 2021

Zelieann R. Craig — Date: Jul 26, 2021

Sean Limesand
Sean Limesand — Date: Jul 26, 2021

Arun K. Dhar — Date: Jul 26, 2021

Final approval and acceptance of this thesis is contingent upon the candidate's submission of the final copies of the thesis to the Graduate College.

I hereby certify that I have read this thesis prepared under my direction and recommend that it be accepted as fulfilling the Master's requirement.

Ravi Goyal — Date: Jul 26, 2021
Ravi Goyal

Acknowledgements

First off, I would like to acknowledge the CALS fellowship and E. Ray Cowden Scholarship funding at the University of Arizona Graduate College. Second, I would like to thank Dr. Ravi Goyal for his encouragement, guidance, and for laying down the groundwork for my research. Third, I would like to give a shout out to Dr. Limesand, Rosa Luna, Dipali Goyal, Alex Pendleton, Serena Sanchez, and Shaira Perez for their contributions to my research and making the ARC an azing place to work. Lastly, I would like to thank Dr. Dhar and Dr. Craig for being a part of my Thesis Committee.

Table of Contents

List of Figures/Tables

Keywords: Adipose, intrauterine, placental insufficiency, fetal growth-restriction, RNAseq, sexually dimorphic, epigenetics

Abstract

Worldwide, fetal growth restriction (FGR) affects 7 to 10% of pregnancies, or roughly 20.5 million infants each year. FGR not only increases neonatal mortality and morbidity but also the risk of obesity in later life. Currently, the molecular mechanisms by which FGR "programs" an obese phenotype are not well understood. Of note, studies demonstrate that FGR females are more prone to obesity as compared to males; however, the molecular mechanisms that lead to FGR are not known. Thus, I hypothesized that FGR causes sexually dimorphic programming of adipocytes by differentially regulating preadipocyte gene pathways. To test the hypothesis, we induced FGR using a sheep model subject to increased ambient hyperthermia. We collected perirenal adipose tissue from male and female near-term FGR and normal weight fetal lambs (N=4 in each group, 16 total). Second-generation RNA sequencing (RNAseq) was conducted on RNA isolated from adipose tissue to examine the differences in gene networks and pathways. For phenotypic results, averages across the four samples for each group were obtained. The current studies demonstrated that male FGR (MFGR) has a significantly greater mean fat globule area than normal-weight male fetus and a greater fat globule area than all other groups. In contrast, there was no significant difference in average fat globule area between female FGR (FFGR) and normal-weight female fetus. A four-way RNAseq comparison demonstrated significant differences in gene expression between FGR and control groups and between sexes. In conclusion, we observed a sexually dimorphic phenotype and gene pathways in response to FGR.

Abstract: 249 words

Body: 11,320 words

CHAPTER 1

The Developmental Origins of Health and Disease

Obesity has emerged as a major health crisis in the USA and around the world. According to the WHO, the prevalence of obesity has been tripled since 1975 [1]. Financially, obesity plays a large part in higher medical costs, decreased productivity, and increased absence from work [2]. With healthcare costs rising every day, the cost of excess health care expenditures takes an enormous toll on individuals. In 2014, globally, the economic impact of obesity was $2.0 trillion US dollars [2]. Additionally, obesity significantly reduces life span and quality of life. It is shown that obesity can decrease life expectancy as much as 5-10 years [3]. Moreover, obesity is related to disorders such as coronary artery disease, arthritis, diabetes, and stroke. Obesity also has a considerable impact on mental health conditions like low self-esteem, mood disorder, and eating disorders [4]. Overall, obesity is immensely impactful on society and requires urgent attention and investigation.

Human epidemiological studies demonstrate that fetal growth restriction (FGR) is a major risk factor for obesity later in life [5]. This has led to the concept of developmental origins of health and disease (DOHaD) and "fetal programming" of obesity and associated metabolic disorders [6] [7]. FGR is defined as fetal weight below the 10th percentile [8] and it has recently been documented that FGR is more prevalent in a group of obese women compared to normal weight women [9]. In the mouse, we have demonstrated that FGR pups are more prone to Obesity and hypertension in a sexually dimorphic manner [10]. Others have also demonstrated similar findings [11, 12]. During the last several years, we have examined epigenetic and genetic mechanisms related to fetal "programming" and DOHaD in response to maternal stress [7] [13] [14] [15] [16] [17] [18] [19] [20] [10] [21].

During the past decade, studies have demonstrated that FGR babies are at significant risk for excessive fat deposition in adipose tissues and rapid catch-up growth in a sexually dimorphic manner [6] [11] [12]. Evidence indicates that adipose tissue consists of three major types of differentiated/mature cells (known as adipocytes): white (WAT), brown (BAT), and beige [22] adipocytes [23]. WAT adipocytes store excess energy as triglycerides, whereas BAT adipocytes expend energy by producing body heat. BAT is plentiful in hibernating mammals and human newborns because it allows for survival in cold temperatures [24]. Studies suggest that beige adipose tissue [22] is a transition state between BAT and WAT [25], and WAT can be converted to BAT and vice a versa. Similar to BAT, BeAT also has the ability to convert accumulated fat into heat [26]. Importantly, along with mature adipocytes, in adipose tissues stored in different parts of the body, there is a population of mesenchymal stem cells like preadipocyte cells [27]. These preadipocytes are a very plastic cell type [28], as they can differentiated into all three lineages: endodermal [29], mesodermal [30], and ectodermal origins [31]. Unfortunately, FGR-mediated programming of preadipocytes and their ability to differentiate into specific mature adipocytes is not well investigated thus creating a significant knowledge gap in our current understanding. Of note, gene pathways and networks involved in "fetal programming" of preadipocytes in response to growth restriction are not known. Thus, in the present study, I tested the hypothesis that FGR differentially regulate preadipocyte and adipogenesis-related gene pathways in male and female sheep offspring.

Methods

All animal studies were reviewed and approved by the Institutional Animal Care and Use Committee (IACUC). Crossbred Columbia-Rambouillet ewes carrying singleton pregnancies were purchased from the University of Colorado Health Sciences Center (UCHSC) as previously reported [32]. The University of Arizona School of Animal and Comparative Biomedical Sciences,, which is accredited by the National Institute of Health, the U.S. Department of Agriculture, and the American Association for Accreditation of Laboratory Animal Care, conducted all animal care and use in compliance with IACUC as well [32]. All experiments were conducted on the following four study groups – near-term control male ovine fetuses (MC), near-term control ovine female fetuses (FC), near-term FGR ovine male fetuses (MFGR), and near-term FGR ovine female fetuses (FFGR) which are described in the following section.

Maternal Heat Stress Model

All studies were conducted on visceral adipose tissue (VAT) obtained from near term ovine fetuses. Pregnant ewes were exposed to ambient hyperthermia (40 ˚C for 12 hours; 35˚C for 12 hours; dew point 22˚C) from 38 ± 1 to 87 ± 1 days of gestation (total gestation in sheep is ~145 days) as previously reported [32]. Increased temperatures cause capillaries in the dermis of ewes to dilate, resulting in increased blood flow to the skin and decreased blood flow through the placenta. The decreased nutrient transfer from mother to fetus caused by this can result in FGR and has been demonstrated in several previous studies [32] [33]. Control fetuses were born from ewes maintained at 22± 1°C and pair-fed an average *ad libitum* feed intake for hyperthermic ewes to avoid feed intake effects. These ambient temperatures were selected because they mimic average January temperatures in Tucson, AZ, where the study took place. An inability to accumulate sufficient postnatal brown adipose in fetal lambs to survive cold winters has been implicated in other maternal heat stress models as well [34]. All ewes were given *ad libitum* access to water and salt [35]. Perirenal adipose tissue was obtained from control and FGR fetuses and RNAs were isolated from adipose tissue for second-generation RNA sequencing (RNAseq). Perirenal fat is a visceral subtype with well-defined boundaries and is covered with a perirenal fascia (Gerota's fascia), which makes it easier to isolate and conduct weight measurement [36]. Fetal weight and perirenal fat weight were recorded for all four groups (Fig. 1-2).

Histology: DAPI and Oil Red-O Staining

First, we prepared a 4% formalin calcium fixative: 30 ml deionized (DI) water, 10 ml 16% paraformaldehyde, and 400 mg $CaCl_2$ and fixed fat tissue on slides for each of the four groups for 5-7 minutes in a -20 C freezer. For DAPI staining, a sufficient amount of DAPI was pipette on the slides to cover the cells, protected from light for 30 minutes before removing the DAPI stain solution (approx. 300nM). The cells were washed 3 times with PBS and imaged on a Leica DMi1 Fluorescent Microscope (Fig. 3). For Oil red-O staining, we prepared a 0.5% Oil red O solution from 2% stock: 12.5 ml 70% ethanol, 12.5 acetone, and 0.5 g Oil red Oil Powder. We diluted the stock solution four-fold by pipetting 400 um acetone, 400 um of isopropanol, and 200 um of the 2% stock solution into a microcentrifuge tube. We fixed the slides with the calcium fixative for 60 minutes and heated the 1 ml of 0.5% Oil red O solution to 60 ˚C. Then, we washed the slides 2x with sterile PBS and briefly with ethanol before adding Oil red-O solution drop wise to prevent overstaining the slide and only selectively stain the triglycerides. After 5 minutes, the Oil red-O solution was removed and the slide was washed again with ethanol and tap water. Slides were placed in ethanol for 10 minutes to remove false positive Oil red O stains before being placed in tap water for 1 min. Finally, slides were washed with slowly running tap water without pouring running tap water directly on tissue. After, cells were visualized for proper staining and pictures were taken to demonstrate lipid accumulation in mature adipocytes from all four groups (Fig. 4).

RNA-isolation

Total RNA was isolated as published in a previous report [37] for RNAseq. Briefly, cells were thawed and homogenized using 3 pulses, 4-6 seconds each. Then, 0.2 mL of chloroform was added per 1 mL of Trizol (0.1 mL per sample). Samples were centrifuged for 15 minutes at 14,000 x g (4 ˚C) and the mixture separated into a lower red phenol-chloroform, interphase, and a colorless upper aqueous solution. The aqueous phase containing RNA was transferred to a new tube very carefully to ensure proteins and other cell components did not contaminate the RNA. Then, 250 µl of isopropanol was added to the aqueous phase (0.5 ml/ ml of Trizol) and incubated for 10 minutes. The sample was centrifuged for 10 minutes at 14,000 x g (4˚C) and the RNA precipitate formed a white gel-like pellet at the bottom of the tube. The supernatant was discarded and the sample was vortexed briefly before centrifugation for 5 minutes at 8000 x g (4˚C). The supernatant was discarded and the RNA pellet was air-dried for 10 minutes. Pellets were resuspended in 20 µl of RNase-free water and measured for quantity (ng/ml) and purity on Nanodrop and Qubit (broad-range) according to 260/280 nucleic acid absorbance ratio before high throughput sequencing or RT-PCR.

RNAseq

Isolated total RNA was sent to University of Arizona Genetics Core Facility for sequencing. Briefly, RNA Samples were measured for quality with an Advanced Analytics Fragment Analyzer *(High Sensitivity RNA Analysis Kit – Catalog # DNF-491 / User Guide DNF-491-2014AUG13)* and quantity with determined with a Qubit RNA quantification kit *(Qubit® RNA HS Assay Kit – Catalog # Q32852)*.

Once quality and quantity were validated, a library was constructed from samples using a Swift RNA Library Kit – (*Catalog # R1024 / Swift Protocol version 3.0*) and Swift Dual Combinatorial Indexing Kit – (*Catalog # X8096*). Upon constructing the library, average fragment size in the library was determined with the Advanced Analytics Fragment Analyzer with the High Sensitivity NGS Analysis Kit – (*Catalog # DNF-486 / User Guide DNF-486-2014MAR10*). Quantity was evaluated with an Illumina Universal Adaptor-specific qPCR kit, the Kapa Library Quantification kit for Illumina NGS – (*Catalog # KK4824 / KAPA Library Quantification Technical Guide - AUG2014*).

After completing final library QC, samples were equimolar-pooled and clustered for sequencing on the NextSeq500 machine. The sequencing run was performed using Illumina NextSeq500 run chemistry *(NextSeq 500/550 High Output v2 kit 150 cycles – Catalog FC-404-2002)*, and data were sent to UAGC Biocomputing Group for further analysis and transmission to the client.

Sequence data was quality validated for RNAseq analysis using FastQC High Throughput Sequence QC Report (FastQC) Version 0.11.9. Sequences with average Phred scores below 34 were discarded resulting in 16 sequences (N=16) with 99-100 base-pair (bp) paired-end reads. Then, we generated a Salmon Version 1.2.1 compatible ENSEMBL genome [38]. Fully annotated genome indices were generated for sheep (Oar_rambouillet_v1.0), cow (ARS-UCD1.2), mouse (GRCm39), and human (GRCh38.p13) using ENSEMBL (v1.0.103) GTF and Toplevel .txt files and alignments were performed using Salmon [38]. Differential gene expression datasets were then created using DESEQ2 Version 1.30.1 package in R-studio. Our DESEQ2 analysis provided log2tranformed expression data normalized to estimate size factors using the “median ratio method” (log2FC) and their respective FDR-adjusted P-values (P-adj).

Following RNAseq analysis, sequences were taken for a PubMed and Gene Expression Omnibus (GEO) [39] Database (NCBI) search for Gene Set Enrichment [40] [40]. The RNAseq data were also used to compare differential gene expression in perirenal adipose tissue across different species (see the following section for details).

Comparative Analysis

First, a large-scale data search was performed for GEO Database [39] high throughput sequencing data from studies investigating BAT gene expression in FGR and sexually dimorphic animal models (Table 3). The studies included are as follows: Study 1 – RNA isolated from VAT in high fat diet (HFD) and standard CHOW fed male and female mice [41]. Study 2 – RNA from four different visceral fat depots in male and female mice: periovarian, epididymal, stromal vascular fraction (SVF) cells fraction, and inguinal adipose tissue (IAT) [42]. Study 3 – RNA from IAT in male and female mice fed CHOW or a HFD [43]. Study 4 – RNA from male and female brown adipocyte induced human pluripotent stem cells (no associated publication). Study 5 – RNA from human subcutaneous adipose tissue (SAT) comparing gene expression between obese males and females (OBM, OBF), Type II Diabetic OBF (T2DOBF), and normal weight females (NWF) [44]. Study 6- RNA from VAT in mice given a high fat/sucrose diet (HFSD) compared to mice given CHOW for 8 weeks. (Table 3) [45]. Study 7 – RNA isolated from VAT in young rats on an ad libitum diet (Y_AL), old AL rats (O_AL), young calorie restricted rats (Y_AL), and O_CR [46]. Study 8 – RNA isolated from VAT comparing gene expression in 5-month-old mice (5mo) and 26-month-old mice (26mo) [47]. Together, these comprise comparative analyses for sex, obesity, FGR, and age-related programming of perirenal adipose tissue.

After retrieving SRA data, we converted SRA files to Fastq files for FastQC analysis before running Salmon alignments to our annotated ENSEMBL sheep genome (v1.0.103). Average mapping of unique reads across all alignments was 76.04%. DESEQ2 differential gene expression data from these GEO datasets were cross-compared with our RNAseq data generated in this study to better understand our sheep model relative to others from a transcriptomic approach. Transcripts from animal studies were converted to human homologs to determine commonly dysregulated genes between different species.

DESEQ2 Analysis

A single R-Studio version 1.3.1073, R-script generating differential gene expression datasets with log2FC and P-adj values was designed and reformatted for all RNAseq data included in the present study [48]. This allowed for gene by gene comparison of our data with comparative studies in the previous section. Using these differential gene expression datasets, a Principle Component Analysis (PCA), a heatmap, and volcano plots were generated in R-Studio using a single R-script reformatted for each dataset (Fig. 7-13). Using the same DESEQ2 datasets, we also generated gene networks on Network Analyst [49] and performed a MEME Suit Analysis [50] (Fig. 14-19).

MEME Suit Analysis

The 5 most significantly dysregulated transcripts from each comparison, along with the 5 significantly dysregulated transcripts shared by MFGR_MC and FFGR_FC comparisons were searched in ENSEMBL genome browser (Tables 1-2, Fig. 6A). Sequences that were 1000 bases upstream of the 5' end were recovered by exporting this sequence data from ENSEMBL. These regions represent promoter regions in these genes. All genes were compiled into a single FASTA .txt file. This .txt file was then pasted into Meme Suit Analysis to discover common motifs between these 20 transcripts and MEME Suit generated 3 conserved motifs, of which one was chosen: ZNF384 (Fig. 19). This motif was chosen because it had the least variability in location and length within 1000 bases upstream of the 5' end. The cis-regulatory element for this conserved motif was determined using the Tomtom search engine in MEME Suit Analysis and can be found on the bottom of Fig. 19.

Pathway Analysis

All of the significantly differentiated transcripts from each comparison were converted to human transcripts (P-adj<0.05). These human transcript IDs along with their respective log2FC values were then uploaded to Network Analyst as gene lists. Minimum networks were generated for Tissue-Specific PPI (Visceral Adipose Tissue=30.0) and the subnetwork with the most nodes was selected for each comparison. Then, significantly enriched KEGG pathways with P-adj values<0.05 were extracted (Tables 11-14). Gene Networks were then generated for each comparison (Fig. 14-18). In large and overcrowded gene networks such as those from between sex comparisons, networks were generated by extracting significantly upregulated and downregulated Gene Ontology: Biological Processes (GO:BP) (P-adj<0.05). GO:BP were not extracted for FGR and control comparisons because the original minimum gene networks were not overcrowded and there weren't any significant GO:BP for males or females. The relevant genes for the most significant KEGG pathway for each network were shown in the top left corner (Fig. 14-18.) The highest P-adj values were reported for each comparison, which signifies the least significantly differentially expressed transcript: MFGR_MC (P-adj=0.00062), FFGR_FC (P-adj=0.032), MC_FC (P-adj=5.8e^{-30}), MFGR_FFGR (P-adj =2.67e^{-27}).

Statistics

A two-way ANOVA test for comparison of means was used to determine significant differences between all four groups for Total Body Weight (TBW), Perirenal Fat Weight, and adipocyte nuclei count. A Two-way test was chosen to distinguish between Sex-mediated and FGR-mediated significant differences (P-Value <0.05). A Bonferroni T-Test for Multiple Comparisons was used to determine if there were any significant differences between any of the four groups in mean fat globule size (P-adj. <0.05). The two-way ANOVA tests demonstrated differences between sexes and differences between FGR and Controls so a T-Test was used to parse out specific differences between each group comparison. P-adj. values in the T-Test and the DESeq2 datasets were adjusted for False Discovery Rate (FDR) to prevent reporting false-positives, which means reporting significantly different mean fat globule sizes or significantly different transcripts that were not actually statistically significant.

Results

Effect of Ambient Hyperthermia on Birth Weight

As demonstrated previously [51], elevated ambient maternal temperature resulted in a significant reduction in fetal birth weight in both male and female fetuses (Figure 1).

Effect of FGR and Sex on Perirenal Weight

To examine functional differences and changes in the "programming" of adipocyte cells, we isolated perirenal fat from all the four study groups: MFGR, FFGR, MC, and FC. We observed that average perirenal fat weight was significantly less in both FGR males and females as compared to normal counterparts (Figure 2A). However, on normalizing the average perirenal fat weight (MC: 14.8 g, MFGR: 8.3 g, FC: 14.1 g, FFGR: 8.7 g) to average TBW (MC: 3683.6 g, MFGR: 1677.3 g, FC: 3109.4 g, FFGR: 1598.7 g), there was no significant difference between FGR and control groups in both sexes (Figure 2B).

Effect of FGR and Sex on Phenotype

Next, we determined the cellular density of perirenal fat by using DAPI nuclear staining and fluorescent microscopy (Figure 3A). As shown in Figure 3B, the nuclear densities of perirenal fat in FFGR fetuses were not significantly different from FC fetuses. Opposingly, the two-way ANOVA statistical test demonstrated that MFGR had significantly lower nuclear density as compared to the FFGR and control male and female fetal lambs.

Upon further histological examination with Oil Red-O staining for lipids, there was a significant increase in fat globule size in perirenal fat from the MFGR group in comparison to the MC group (Figure 4A-E). However, average fat globule size in FFGR was not significantly different than FC (Figure 4F).

Effect of Sex on Gene Expression

Changes in adipogenesis are associated with differential gene expression in perirenal adipose tissue from male and female fetal lambs. The 5 most significantly dysregulated transcripts between sexes are listed with their respective gene expression data in Table 1. As shown in Table 3 and Figure 6-7, there was a significant effect of FGR and sex on gene expression. There were 1635 significantly upregulated and 1466 significantly downregulated transcripts in MFGR compared to FFGR. There were 1583 significantly upregulated and 1587 significantly downregulated transcripts in MC compared to FC (Table 3). Of these, 2029 (42.7%) transcripts were shared between FGR and control male and female fetal lambs (Figure 7B).

Effect of Intrauterine Growth Restriction on Gene Expression

Differences in adipocyte differentiation are demonstrated by differential gene expression in perirenal adipose tissue between FGR and controls. The 5 most significantly dysregulated transcripts between FGR and controls are listed with their respective gene expression data in Table 2. There was a total of 343 significantly upregulated and 203 significantly downregulated transcripts in perirenal adipose tissue MFGR compared to MC. There was a total of 9 significantly upregulated and 4 significantly downregulated transcripts in perirenal adipose tissue from FFGR compared to FC (Table 3). Of these, only 5 significantly dysregulated transcripts (0.9%) were shared between sexes (Figure 7A).

Comparative Analysis

Effect of Sex

In study 1 (GSE137022), there were 6920 significantly upregulated and 3559 significantly downregulated transcripts in MHFD compared with FHFD mouse VAT (Table 5) [41]. On comparison of the sex-related differentially expressed genes identified in our RNAseq data with study 1 (Table 7-8), MHFD shared 23 and 25 significantly upregulated transcripts with MFGR and MC, respectively, and only 17 and 14 with FFGR and FC, respectively (P-adj.<0.5) (Tables 7-8). In the same study, differential gene expression between MCHOW and MHFD was compared our RNAseq data, revealing MCHOW shared 30 and 15 significantly upregulated transcripts with MFGR and MC, respectively, and only 1 and 0 with FFGR and FC, respectively. MHFD shared 35 and 47 significantly upregulated transcripts with MFGR and MC, respectively and only 0 and 2 with FFGR and FC, respectively.

In study 2 (GSE121836), there were 3 different adipose tissue types compared between male and female mice: gonadal, SVF cells, and inguinal. There were 5648 significantly upregulated and 2721 significantly downregulated transcripts in epididymal compared to periovarian adipose tissue, 12582 significantly upregulated and 15457 significantly downregulated transcripts in MSVF vs FSVF cells, and 5832 significantly upregulated and 6092 significantly downregulated transcripts in male inguinal compared to female inguinal adipose tissue (Table 5) [42]. Of these, there were 22 and 28 significantly upregulated transcripts shared between epididymal and MFGR and MC adipose tissue, respectively, compared to 21 and 15 shared with FFGR and FC, respectively. Further, there were 9 and 7 significantly upregulated transcripts shared between periovarian and FFGR and FC adipose tissue, respectively, compared to 1 and 3 shared with MFGR and MC. There were 326 and 245 significantly upregulated transcripts shared between MSVF cells and MFGR and MC, respectively, compared to 170 and 190 shared between MSVF and FFGR and FC, respectively. Further, there were 283 significantly upregulated transcripts shared between FSVF cells and FFGR compared to 175 shared between FSVF and MFGR adipose tissue. Finally, there were 171 significantly upregulated transcripts shared between male inguinal and MFGR adipose tissue compared to 121 shared between male inguinal and FFGR adipose tissue. There were 96 significantly upregulated transcripts shared between female inguinal and FFGR adipose tissue compared to 70 significantly upregulated transcripts shared between female inguinal and MFGR adipose tissue (Tables 7-8).

In study 3 (GSE1511358), there were 1421 significantly upregulated and 2190 significantly downregulated transcripts in male compared to female inguinal mouse adipose tissue (Table 5) [43]. Of these, there 23 significantly upregulated transcripts shared between ad libitum female and FFGR adipose tissue and 16 shared between ad libitum female and MFGR adipose tissue (Tables 7-8).

In study 4 (GSE168387), there were 26949 significantly upregulated and 22109 significantly downregulated transcripts in male compared to female human brown adipocyte-induced pluripotent stem cells (Table 5) (No associated publication).

In study 5 (GSE166047), there were 425 significantly upregulated and 589 significantly downregulated in SAT from obese males (OBM) compared to obese females with Type II Diabetes

(T2DOBF) (Table 5-6) [44]. Of these, 7 significantly upregulated transcripts were shared between T2DOBF and FFGR and FC compared to 1 and 2 shared between T2DOBF and MFGR and MC, respectively. In the same study, there were 3094 significantly upregulated and 2981 significantly downregulated transcripts in OBM compared to normal weight females (NWF). Of these, there were 31 and 30 significantly upregulated transcripts shared between OBM and MFGR and MC, respectively, compared to 13 shared between OBM and both FFGR and FC. Further, there were 44 and 47 significantly upregulated transcripts shared between NWF and FFGR and FC, respectively, compared to 23 and 13 shared between NWF and MFGR and MC, respectively (Tables 7-8).

Effect of Obese/FGR Models

In study 5, T2DOBF shared 7 significantly upregulated transcripts with FFGR, 5 with FC, 2 with MC, and 1 with MFGR and NWF shared 47 significantly upregulated transcripts with FC and 44 with FFGR (Table 9-10).

In study 6 (GSE112947), there were 11291 significantly upregulated and 9707 significantly downregulated transcripts in MCHOW mouse VAT compared to MHFSD mouse VAT (Table 6) [45]. Of these, there were 63 significantly upregulated transcripts shared between MHFSD and MFGR compared to 34 significantly upregulated transcripts shared between MCHOW and MFGR (Tables 9-10).

In study 7 (GSE137869), there were 1649 significantly upregulated and 2073 significantly downregulated transcripts in Y_AL compared to O_CR rat VAT, 2861 significantly upregulated and 3453 significantly downregulated transcripts in Y_AL compared to O_AL rat VAT, and 1700 significantly upregulated and 2022 significantly downregulated transcripts in O_AL compared to O_CR rat VAT (Table 6) [46]. Of these, O_CR shared 36 and 6 significantly upregulated transcripts with MFGR and MC, respectively, compared to 14 and 19 significantly upregulated transcripts shared between Y_AL and MFGR and MC, respectively. O_AL shared 58 and 15 significantly upregulated transcripts with MFGR and MC, respectively, compared to 37 and 30 significantly upregulated transcripts shared between Y_AL and MFGR and MC, respectively. Lastly, there were 19 and 71 significantly upregulated transcripts shared between the WT rat group and MFGR and MC, respectively, and O_CR rats shared 31 significantly upregulated transcripts with MFGR (Tables 9-10).

Effect of Age

In study 8 (GSE124772), there were 478 significantly upregulated and 636 significantly downregulated transcripts in 5mo vs. 26mo old rats [47] (Table 6). Of these, 5mo shared 4 and 2 significantly upregulated transcripts with MFGR and MC, respectively, compared to 0 and 2 with FFGR and FC, respectively. Twenty six month sample shared 2 and 2 significantly upregulated transcripts with MFGR and MC, respectively, compared to no difference in gene expression with FFGR and FC, respectively.

DESEQ2 Analysis

The PCA demonstrates that the samples are clustered closely within their respective groups with the exception of one CF sample which appears to be more closely related to FFGR than the rest of the CF samples. Both sexes were highly clustered. There were no outliers (Figure 8, Figure 14). There were far greater significantly differentiated transcripts in volcano plots comparing sexes than those comparing FGR and controls, as demonstrated by the number of red dots in each plot (Fig. 9-13). Furthermore, the 5 most significantly differentiated transcripts between sexes in FGR and control groups had much lower P-adj values than the 5 most differentially expressed transcripts between FGR and control males and females. The heatmap demonstrates in-between group and sex differences based on up (green) and downregulation (red) of transcripts in each sample (Fig. 14). Genes and groups were clustered in dendrograms according to Euclidian distance from the median. The heatmap identifies the CF group outlier in the PCA: CF_B (Fig. 14, Supplementary Table 1). The 5 most significantly differentially expressed genes from each group comparison were chosen for Meme Suit Analyses to determine conserved binding motifs for transcription regulatory elements (Table 1, Fig. 15) ($P\text{-adj}<10e^{-10}$, $\log2FC>|1.5|$).

Meme Suit analysis:

As shown in Figure 19, we found a 49 bp common motif, ZNF384, in the 18 transcripts of interest which is present in the promoter region of several transcripts of interest (see methods section for details). The promoter regions of the of the 5 differentially expressed transcripts between sexes demonstrate a common motif sequence of 35 bp, ZNF263. In this 35 bp region we identified binding sites for three novel transcripts, NDUFB3 and MICOS10 (Fig. 20). The promoter regions of the 5 differentially expressed transcripts between MFGR and MC demonstrate a common motif sequence of 44 BP, FOXK1_DBD. In this 44 bp region, potential binding sites for GREB1 and AADAC were identified (Fig. 21). The promoter regions of the 5 differentially expressed transcripts between FFGR and FC demonstrate a common motif sequence of 50 bp. In this 50 bp region, we identified binding sites for AADAC, MACROD1, GREB1, TRIP12, HSPA6, and one novel transcript (Fig. 22).

Pathway Analysis:

None of the top canonical KEGG pathway enrichments were significant in the FFGR_FC comparison and there was only one significant KEGG pathway enrichment in the MFGR_MC comparison, the FoxO signaling pathway (P-adj =0.029, Tables 11-12). As for between sex comparisons, Tables 13-14 represent significantly enriched pathways (P-adj <0.05). The most significantly enriched pathways for MFGR_MC, FFGR_FC, MC_FC, MFGR_FFGR upregulated, and MFGR_FFGR downregulated are FoxO signaling pathway, estrogen signaling pathway, endocrine resistance, small cell lung cancer, and the PI3-Akt signaling pathway, respectively (Fig. 14-18). Genes involved in these processes are shown in the top left of each gene network. Our gene networks demonstrate which genes play a role in dysregulated pathways by identifying key transcriptional regulators, protein-protein interactions, and significant GO:BP relationships (Fig. 14-18).

CHAPTER 2

The Thrifty Phenotype

Fetal growth restriction is often followed by postnatal catch-up growth, which is associated with adulthood metabolic and cardiovascular disorders. This phenomenon is detailed in the “Thrifty

Phenotype Hypothesis” where a lack of placental nutrition from the mother may confer a fitness advantage for the fetus, which becomes detrimental when the postnatal environment does not mimic in-utero resource scarcity. In the case of placental insufficiency, adipose tissue is reprogrammed to conserve energy, characterized by larger WAT depots and lipid accumulation, abnormal BAT morphology, and dysregulation of brown adipogenesis. This leads to overall greater triglyceride storage and an inability to burn as much fat in adulthood, especially when the postnatal environment has excess of food resources [5]. Our results support “The Thrifty Phenotype Hypothesis” in a sexually dimorphic manner.

Our sheep maternal heat stress model results in fetal growth restriction, validating our maternal ambient hyperthermic chamber as a means to produce placental insufficiency (Fig. 1). We propose the lack of nutrient transfer from the mother occurs due to increased maternal energy expenditure when temperatures are around 104° F [52]. Heat stress dilates endothelial cells causing increased blood flow to the skin at the expense of maintaining blood flow to the fetus through the placenta. This heat stress model was proposed based on higher observed mortality rates in lambs born in warmer seasons [51]. Other models of placental insufficiency include maternal oxygen deprivation and maternal diet restriction but these are associated with higher rates of morbidity than elevated ambient temperatures and can cause other reproductive complications in fetal lambs [53].

Perirenal fat has been identified as a major target for in-utero reprogramming during maternal stress. It has previously been shown that FGR and HFD-programmed adipose tissue enhances lipogenesis and adipocytes proliferation [54]. However, we noticed significantly decreased perirenal fat weights in the FGR groups compared to controls (Fig 2A). Differences in perirenal fat weight between samples can have an effect on genotype and phenotype. Upon normalization of perirenal fat weights to total body weights (TBW), there were no significant differences in perirenal fat weight between FGR and controls suggesting any phenotypic or gene expression group differences are not an effect of perirenal fat weights (Fig. 2B). It has been proposed that reprogramming of adipose tissue can be attributed to early induction of adipogenesis transcription factor, Peroxisome Proliferator

Activated Receptor Gamma (PPAR- γ), along with a number of other adipogenic biomarkers whose expression are dysregulated under limited or excess nutrients.

Effect of Sex and FGR on Adipocyte Proliferation and Fat Storing Capacity

Our data is consistent with previously reported increases in lipogenesis, decreased lipolysis, adipocyte proliferation and fat globule storage in IUGR compared to control groups and in females compared to males [54] (Figure 3, Figure 4). FFGR had the largest average fat globule area despite there being no significant difference between FC and FFGR perirenal average fat globule size. MFGR had significantly greater average fat globule area than MC though, suggesting that FC has greater average fat globule area than MC (Fig. 4). This data demonstrates differences in fat storage capacity between sexes and between FGR and controls, where it appears female FGR adipose tissue may become remodeled during placental insufficiency to conserve more energy by accumulation of excess triglycerides in adipocytes. These triglycerides can then be accessed as energy reserves during fasted states by fatty acid mobilization [55].

Due to maternal undernutrition in the case of FGR, the fetus enters a fasted state in utero, causing lower levels of insulin secretion. These low plasma insulin levels mean less antilipolytic effects, because insulin is necessary for conversion of glucose into glycerol in the liver. Due to the unavailability of glycerol being transported from the liver to adipose tissue, there is a build-up of intracellular non-esterified fatty acids (NEFAs) rather than triglyceride storage, which requires 3 fatty acids and glycerol. NEFAs activate PPAR-γ and leptin receptors which drive adipogenesis. Overactivation of these pathways can lead to adipocyte hypertrophy and hyperplasia [56]. In support of these findings, a study on adipogenesis development during 24 hours post parturition shows low plasma insulin levels in females and high plasma insulin levels in males [57]. It is thus possible that the mechanism for increased lipid content and fat storage in IUGR is the same for this finding in adipose tissue from female compared to male fetal lambs.

Previous studies have shown that body fat in humans and other mammals are significantly different between males and females [58] [59]. In general, women have more SAT and men have more VAT and lipolysis rates in SAT are lower than in VAT [58] [60]. This discrepancy is associated with increased levels of postprandial insulin and free fatty acids (FFA) in men [61]. Thus, FFGR and FC may exhibit decreased lipolysis compared to their male counterparts because they have less VAT. This would suggest the risk of FGR-programmed adiposity may be lower in males than females in concordance with most recent literature, as women appear to be more susceptible to obesity in adulthood than men on average [7]. In support of these findings, obese men have higher rates of lipolysis than healthy individuals and obese women. This causes an overaccumulation of FFA in the liver due to increased hydrolyzation of TG, often leading to increased hepatic glucose production, hyperinsulinism, and other symptoms of metabolic syndrome [62].

Sex-Mediated Programming of Adipose Tissue

The present study has identified the top 5 most significantly dysregulated transcripts in perirenal adipose tissue between sexes, which were shared between FGR and control groups. There were 3 novel transcripts and two transcripts encoded by the following human orthologs, MICOS10 and NDUFB3 (Table 1). Downregulation of MICOS10 results in diminished mitochondrial function, which is a pathological hallmark of neurodegenerative conditions, muscular dystrophies, myopathies, and obesity and diabetes [63]. Considering MICOS10 is downregulated in males compared to females in both groups, MICOS10 expression might promote adipogenesis and/or fat storing capacity in females. Thus, overexpression of MICOS10 in females may cause increased lipid content in females, programming a perirenal fat phenotype that is more prone to obesity in both groups.

NDUFB3 (NADH:Ubiquinone Oxireductase Subunit B3) is a gene that encodes an NADH dehydrogenase subunit, which is the first enzyme of the electron transport chain (ETC) of the mitochondria. A recent study showed that reduced NDUFB3 expression is associated with FGR children and variable adulthood metabolic phenotype [64]. It is possible that NDUFB3 expression is negatively correlated with uncoupling protein 1 (UCP-1) expression because UCP-1 facilitates oxidative uncoupling by leaking protons into the inner mitochondrial matrix, which would decrease the proton motive force that is driving ETC activity. Downregulation of NDUFB3 may thus, be an epigenetic adaptation to FGR that occurs in males but not in females, where males have greater UCP-1 expression in brown fat or have a higher ratio of brown to white fat. This would promote fat burning, as energy would be released as heat by the proton motive force through the UCP-1 channel rather than being stored as ATP through the ETC [64]. The three novel transcripts are also of particular interest but more research is necessary before any conclusions can be made about these.

The three novel transcripts are also of particular interest but more research is necessary before any conclusions can be made about these. However, it is important to note SARNP expression downregulates E-Cadherin and promotes progression of breast cancer in humans, which is often associated with obesity [65]. DACT1 is a preadipocyte gene that decreases during adipogenesis. Furthermore, knocking down DACT1 inhibits adipogenesis by activating the WNT signaling pathway way and overexpression of DACT1 promotes adipogenesis by increasing expression of Sfrps and reducing expression of WNTS in mice [66]. Finally, overexpression of GOLM2 is associated with breast and ovarian cancer in humans, demonstrating the role that sex and FGR may play in cancers as well. Taken together, these findings are congruent with our phenotypic data because each of these transcripts were downregulated in males compared to females in both FGR and Control groups and we have shown decreased adipogenesis in males compared to females (Fig. 4). These results suggest that males may be less susceptible to adulthood development of metabolic disorders and breast or ovarian cancer than females in both groups.

RNAseq data from the current study has revealed greater significant differential gene expression between MFGR and MC compared to FFGR and FC, suggesting more dysregulated pathways or genetic adaptations to dysregulated pathways resulting from FGR in males than females. There was also much greater differential gene expression between sexes in both groups than between FGR and controls in either sex (Table 3, Fig. 5). Furthermore, there were substantially more significantly dysregulated genes between sexes that were shared between control and FGR groups than there were significantly dysregulated genes between FGR and control groups shared between sexes (Fig. 6). This suggests that many of the same genes regulate adipose tissue development in control and FGR males. The same goes for females. However, the genes that program perirenal adipose tissue in FGR and control females most likely do not program adipose tissue in FGR and control males and vice versa. This is important for the biomedical field because research on drug development for treating obesity in females should target different genes than those developed to treat obesity in males.

Within these Venn diagrams, the 5 significantly dysregulated transcripts that were shared between MFGR_MC and FFGR_FC are of particular interest (Fig. 6A). There were 4 that were respective of sex (overlapping with sex comparisons) and 1 that was irrespective of sex (no overlap): ITGB4-201, PMPCA201, MACROD1-201 and one novel transcript (ENSOART00020005697.1), and HSPA6-201, respectively (Fig. 5). HSPA6-201 is part of the Heat Shock Protein Family A complex with a highly enriched cellular response to heat stress. This would make sense that this is dysregulated between FGR and control irrespective of sex because FGR fetuses were born from ewes exposed to heat stress on gestational day 75. Thus, the response in adipose tissue to heat stress is under regulation of HSPA6-201 in both males and females. ITGB4 has been identified as a known risk factor for obesity-related carcinogenesis in endometrial cancer, particularly in premenopausal women [65]. Considering its sexually dimorphic role in endometrial cancer, dysregulation of the transcript ITGB4-201 in the present study reveals a potential role in differentially programming adipose tissue in FGR males and females.

Based on the PCA and the heatmap (Fig. 7 and Fig. 8), the samples from the present study are clustered well within their respective groups and especially within their sexes. The heat map demonstrates that significantly upregulated transcripts (green) in males were significantly downregulated (red) in females and vice versa. Of note, there is one sample point in our PCA that is relatively farther in distance from the rest of the CF samples than the IUGRF samples. This sample point is identified in the heatmap as CF_B in the heatmap. Considering CF_B is still clustered closely with the rest of the female samples, it is not an outlier. The dendrogram clustering of samples suggests the same finding on the x-axis of the heatmap as well, which is further evidence that sex plays a much greater role in programming adipose tissue than FGR does.

Our volcano plots illustrate the same finding (Fig. 9-13). There were only 3 significantly dysregulated transcripts in MFGR compared to MC and only 1 significantly dysregulated transcript in FFGR compared to FC (log2FC>|1.5|, P-adj<10e^{-10}). One of the 2 significantly upregulated transcripts in MFGR compared to MC was novel and the other two were GREB-201 and PCK2-201 which will be discussed in the following section. However, there were 197 significantly dysregulated transcripts between FGR males and females and 177 significantly dysregulated transcripts between control males and females (log2FC>|1.5|, P-adj<10e^{-10}).

The comparative analysis shows that many of these significantly dysregulated transcripts are conserved across different species of mammals, including humans suggesting growth restricted fetal lambs are a strong model for placental insufficiency, FGR, and obesity (Tables 5-8). Thus, the significantly dysregulated transcripts in this study are unique and essential meaning they do or have in the past conferred a fitness advantage for both sexes. It is possible that the mechanisms that regulate adipogenesis in FGR and control males reduces the risk of obesity compared to FGR and control females based on our phenotypic results. Thus, a close analysis of conserved dysregulated pathways was warranted to reveal therapeutic targets for sex-mediated FGR programming of obesity in humans.

Pathway analysis revealed significant enrichment of the PI3K/AKT signaling pathway in the MC_FC and MFGR_FFGR comparisons (P-adj<3.91e^{-7} and <3.77e^{-8}, respectively) (Tables 13-14, Fig. 18). Based on recent literature, this pathway is essential for normal metabolism and its imbalance contributes to development of T2D and/or obesity. Damage or dysregulation of this pathway in a number of tissues causes insulin resistance, which further exacerbates the PI3K/AKT pathway, creating a vicious cycle [65]. Particularly in the MFGR_FFGR comparison, genes involved in the PI3/AKT pathway are heavily downregulated in males compared to females, such as YWHAE (log2FC=-2.66) and GNG5 (log2FC=-1.28). Based on physiologic roles of the PI3/AKT pathway, these genes most likely mediate growth factor signals during organismal growth and essential cell processes, like glucose homeostasis, lipid metabolism, protein synthesis and cell proliferation and survival [66].

Other pathologies listed in Tables 13-14 represent differentially expressed pathways between sexes but PI3K/AKT signaling pathway is of particular interest in the field due to its role in programming adipose tissue via prenatal and postnatal lipid biosynthesis and inhibition of lipolysis during feeding, fasted, and fed states. Fatty acid synthase, cholesterol related genes, and FOXO1 are regulated by the substrate, SREBP, because it modulates expression of the rate limiting adipose triglyceride lipase (ATGL). In the feeding state, SREBP-1c is under regulation by four AKT-activated pathways: stimulation of liver X receptor (LXR) which promotes SREBP1-c transcription, enhancement of mTORC1 activation of SREBP-1c transcription, mTORC1 inhibition of Lipin-1 which decreases nuclear SREBP-1c half-life and activates S6K1, promoting SREBP-1c maturation, and suppression of insulin induced gene 2A (INSIG2A), which also promotes SREBP-1c maturation of precursors into nuclear forms [66]. In the fasted state, lipolysis is acutely induced by β-adrenergic signaling, causing accumulation of cAMP and phosphorylation of Hormone-Sensitive Lipase (HSL) by PKA and perilipin. In the fed state, PI3K/AKT inhibits PKA, which is antilipolytic. Independent of AKT, PI3K modulates adipocyte lipolysis by directly controlling PKA. AKT however regulates FoxO1 through three pathways that reduce expression of ATGL. ATGL activation is required for activating interferon 4 (IRF4) induction of lipolysis. Lastly, phosphorylating phosphodiesterase 3b (PDE3B) decreases intracellular cAMP levels and PKA activity, ultimately inhibiting lipolysis in adipocytes. We speculated this inhibition of lipolysis postnatally occurs in males at a greater rate than women due to higher levels of insulin at birth, resulting in lower intracellular NEFAS and thus, decreased activation of PPAR-y. The same process occurs on gestational day 75 when maternal heat stress is induced. These represent some of the pathways that are differentially expressed between males and females resulting in increased lipolysis during prenatal and postnatal fasted states as a result of FGR that may decrease susceptibility to obesity. However, validation of dysregulated genes in these pathways by qPCR and Western Blot is required before making concrete conclusions on their role in sex-mediated programming of adipose tissue.

Fig. 16-18 begins to paint an overall picture of prevalent genes and protein interactions that are differentially expressed in males and females providing lists of sex and obesity related gene targets and their relationships. Following qPCR and Western Blot validation, our functional analysis describes targets for *in vitro* and *in vivo* mouse KO and knock-in studies. Considering the ubiquitous nature of the PKI3/AKT signaling pathway, it might be of benefit to the field to investigate tissue-specific KO studies to understand phenotype and deeper genetic analysis of different tissues. The essential role of this signaling pathway in normal metabolism suggests that a whole genome KO might not generate viable and/or fertile offspring, a major limitation of using upstream targets for KO studies.

This data begs the question, by which mechanisms does FGR alter so many genes in such an organized manner? In order to address this question, we examined promoter regions of the altered genes by group comparisons, isolating FGR and control and sex comparisons. Cis-regulatory and trans-acting factors appear to lead to the dysregulation of several genes between sexes belonging to the canonical and functional pathways mentioned in the current study (Fig. 20). We identified the Zinc-like finger, ZNF263, as a binding site in the promoter region of the most dysregulated genes from our sex comparisons. This suggests sex-mediated programing of ZNF263 expression leads to increased adipogenesis and fat storing capacity in FGR and control females compared to FGR and control males, respectively. Further experiments are necessary, however, to establish the role of ZNF263 in regulating pathways such as PI3/AKT, and its role in obesity. The present report provides strong rationale for such studies [67].

Differences in adipose tissue between males and females is largely attributed to sex hormone differences. Past studies have demonstrated that ovariectomized female mice had increased weight gain and metabolic impairment, which was nearly recovered to wild-type phenotype when estrogen was replaced [68] [69]. Furthermore, estrogen receptor alpha (ERα) deletion from adipocytes increases visceral adiposity and the susceptibility to metabolic syndrome [70]. 17ß-estradiol replacement in ovariectomized WT mice prevents obesity, which is not observed in ERα-deficient mice [71]. Androgens also play a role in adiposity, demonstrated by improved insulin sensitivity in tissue-specific AR overexpressed mice and increased adiposity in Androgen Receptor Knockout (AR-KO) mice [72]. In support of the deleterious role of androgens in BAT development, decreased energy expenditure and adiposity, increased levels of triglycerides, and impaired metabolism was observed when testosterone was replaced in castrated mice. Finally, BAT-mediated thermogenesis is upregulated by estrogen. While there is generally more estrogen in females, desensitization effects may cause increases in estrogen levels in males to have an overall greater effect in BAT in men than women. This rise in activity of BAT that increases body temperature is negatively associated with weight gain [73]. Together with our findings, this demonstrates the role of circulating and local sex hormones secreted from adipose tissue in sexually dimorphic BAT structure, distribution, and function [74].

Sex differences in BAT inflammation has also been well studied. VAT leukocyte accumulation and activation are strongly correlated with metabolic dysfunction as well, suggesting sex differences in VAT inflammation as well [75]. However, more data is necessary to make clear the physiologic association between VAT inflammatory cytokines and lipid content. Further, female animal models tend to expand adiposity by anti-inflammatory mechanisms, while male animal models experience increased adipocyte death by macrophage infiltration which protects against obesity [58]. Adipose tissue subject to metabolic inflammation causes abnormalities such as glucose intolerance so it is possible that increased adiposity and adipose tissue inflammation may be an underlying cause of insulin signaling dysregulation in obese individuals [74]. Furthermore, VAT has more macrophages than SAT, which produce proinflammatory cytokines such as interleukin-6 (IL-6) and tumor necrosis factor-alpha (TNF-α) and less adiponectin. This can cause loss of function in endothelial cells and atherosclerosis as a result of cytokine-induced insulin resistance playing a prominent role in diabetes as well [76].

In addition to inflammation-related remodeling, sympathetic innervation differs between sexes. As a result, there is female-specific protection against metabolic disease where brown adipocytes are induced in gonadal VAT [77]. A previous study in humans revealed that catecholamine-mediated leg FFA release, FFA release by upper body, basal fat oxidation, and postprandial fat storage are significantly greater in adipose tissue obtained from males than females [78]. In vivo, catecholamine FFA release activates greater epinephrine and isoproterenol secretion in males than females. This stimulates FFA release, correlating with enhanced lipolysis rates in males. Secondly, there are elevated rates of FFA release in SAT from males than from females, resulting in decreased antilipolytic effects with meal ingestion. Thirdly, basal fat oxidation is lower in females compared to males, another factor leading to lower levels of circulating FFA and slower metabolic rates in women [78].

Last but not least, there are X and Y chromosome differences that could lead to epigenetic changes. A recent plethora of primary and review literature has examined methylation patterns, micro RNAs (miRNAs), and lincRNAs that lead to sexually dimorphic phenotypes in the case of FGR [79]. miRNAs regulate gene expression by increasing degradation or disrupting translation [80]. miRNAs are enriched in X chromosomes, increasing the likelihood that miRNAs are not silenced by X-linked inactivation in females [81]. This may lead to suppression of miRNA biomarkers for immunosuppression, causing increased autoimmunity which predisposes individuals to autoimmune diseases [82]. A similar effect is seen in differential gene expression of metabolic biomarkers by sex. Specifically, miRNAs have been observed to enhance differentiation rates in adipocytes and modulate metabolic and endocrine pathologies [83]. It has been also recently discovered that some sex-biased miRNAs play roles in adipogenesis [84]. That being said, the overwhelming majority of literature on miRNAs involved in adipogenesis has been investigated in male animal models. Similar to adipokines, adipocytes secrete miRNAs into the bloodstream. Thus, they have inter-tissue and organ endocrine-like communication that may serve as therapeutic targets for dysregulation of adipocyte differentiation as well [85].

FGR-mediated Programming of Adipose Tissue

The present study has identified the 5 most significantly dysregulated transcripts in perirenal adipose tissue between FGR and control, of which none were shared between sexes. In males, there were two novel transcripts and three transcripts encoded by the following human orthologs, PCK2, AADAC, and GREB1 (Table 2). More research investigating these two novel transcripts would benefit the field considering their abnormally high fold-change values. In females, there was one novel transcript encoded by the human ortholog, HSPA6, and 4 transcripts encoded by the following human orthologs, SEC24B, SIMC1, SEMA7A, and TRIP12 (Table 3).

PCK2 (Phosphoenolpyruvate Carboxykinase 2) encodes PEPCK-C, along with PCK2-201 from our dataset, which is the key enzyme of gluconeogenesis in the liver and kidney suggesting PCK2-201 plays a role in blood glucose levels as well. It is also detailed in the Thrifty Phenotype Hypothesis that permanent changes in insulin signaling pathways is a result of poor fetal nutrition [6]. Upregulation of PCK2-201 in MFGR compared to MC is consistent with the Thrifty Phenotype sequalae and high rates of insulin resistance observed in obese patients. In further support of this, mouse models of tissue-specific overexpression of PEPCK-C has resulted in T2D as well as obesity, lipodystrophy, fatty liver, and death by increased fatty acid re-esterification. Increased levels of intracellular fatty acids in adipose tissue is associated with increased activation of PPAR-y and leptin expression so fatty acid re-esterification may be the cause of adipocyte hyperplasia observed in FGR. AADAC (Arylacetamide deacetylase) regulates triglyceride lipase activity in the liver, which also increases intracellular fatty acids. On top of this, KO of AADAC in human differentiated vascular smooth muscle cells demonstrated increased triglyceride storage and overall lipid droplet content. Dysregulation of GREB1 (Growth Regulating Estrogen Binding-1) is associated with poly-cystic ovarian syndrome [86] and PCOS patients have an increased risk of becoming obese [86].

Increased expression of SEC24B is associated with morbid obesity and upregulation of SEC24B-201 as observed in FFGR compared to FC. MACROD1 expression promotes an inflammatory response by activating Rac1-MAPK/ERK pathways and reduces insulin-stimulated glucose uptake in adipocytes by impairing the insulin stimulated receptor signaling pathway. Furthermore, MACROD1 expression causes hypercholesterolemia, which occurs in obese people [89]. SIMC1 is associated with the disease SOTOS Syndrome 1, which is characterized by overgrowth during childhood. Growth-restricted fetuses undergo rapid catch up growth [90], which increases the risk of SOTOS Syndrome 1. While SIMC1 dysregulation may not be directly related to obesity, upregulation of SIMC1 in females may be a result of increased activation of rapid catch-up growth-related genes. Dysregulation of PMPCA is associated with mitochondrial dysfunction which is a hallmark of obesity and other metabolic disorders [91].

Increased expression of SEC24B is associated with morbid obesity and upregulation of SEC24B-201 was observed in FFGR compared to FC. SIMC1 is associated with the disease SOTOS Syndrome 1, which is characterized by overgrowth during childhood. Growth-restricted fetuses undergo rapid catch up growth [87], which increases the risk of SOTOS Syndrome 1. While SIMC1 dysregulation may not be directly related to obesity, upregulation of SIMC1 in females may be a result of increased activation of rapid catch-up growth-related genes. SEMA7A is found in lymphocytes and erythrocytes and its expression is associated with decreased bone marrow density, which is a hallmark of FGR. Part of the reason growth-restricted fetuses do not grow to normal weight during pregnancy is because osteogenesis is impaired at the expense of the resources contributed to maintaining energy homeostasis and adipose tissue development in response to placental insufficiency. A recent study showed that the haploinsufficiency of E3 ubiquitin-protein ligase gene TRIP12 causes intellectual disabilities such as autism spectrum disorders, speech delay and dysmorphic features. In this study, 4 of the 7 children that presented with TRIP12 deficiency had obesity which might explain why TRIP12 was significantly downregulated in FFGR compared to FC [88]**.** Despite there being very few significantly dysregulated transcripts in FFGR compared to FC, these genes along with the 5 most significantly dysregulated transcripts in MFGR compared to FC may reveal differences between male and female FGR-mediated programming of adipose tissue (Table 4).

By comparing our FGR model to diet-induced models for obesity, the present study demonstrated differential gene expression between FGR/obese models and controls and between young and aging mice (Table 6). Furthermore, there was an overall trend where gene expression in adipose tissue from obese, T2D, and aging models in mouse, rat, and humans resembled the FGR groups from our study more than the controls groups from our study. This suggests that the transcripts that regulate FGR also program obesity, aging-related effects, and T2D and are conserved across species of mammals. If dysregulation of these transcripts is a result of FGR-mediated programming of adipose tissue, it is possible these transcripts are dysregulated by placental insufficiency or they are adaptations to poor fetal nutrition that have at some point conferred a postnatal fitness advantage for the fetus. Otherwise, these dysregulated pathways would not have been under selected and would not be evolutionarily conserved across different species. Of importance, both FGR and HFD contribute to susceptibility to obesity similarly and the risk of obesity increases with age [7]. Furthermore, BAT decreases with obesity and age which is of particular interest of the current study due to its role in energy homeostasis and weight regulation [89]. Finally, considering the typical life span of lab mice, the young and aging groups used in our comparative analysis accurately reflect effects of aging (Table 4). This would be comparable to a study on 25-year-old vs. 65-year-old humans but it would be speculation to suggest human and mice aging-related effects are linear.

As previously mentioned, the stark differences in gene expression between sexes was not observed when comparing gene expression between FGR and controls (Fig. 9-13). This is yet another example of the prominent role that sex plays in programming adipose tissue in comparison to the role of FGR in programming adipose tissue. Considering there are far fewer genes under regulation by FGR than there are under sex-mediated regulation, we can conclude that sex plays a far more complex role in programming adipose tissue than FGR. Thus, the present study may reveal more about sex-mediated programming than FGR and it represents a field that is particularly understudied. Recent literature has just begun to scratch the surface of FGR mediated differences in perirenal adipose tissue phenotype and gene expression and the potential for viable treatments for obesity, of which diet-related treatments dominate.

For the MFGR_MC comparison, the only significantly enriched KEGG pathway is the FoxO signaling pathway (Table 11, Fig. 14). This pathway is highly prevalent in cancer but has recently been shown to have a dual role in metabolic disorders, such as obesity and diabetes. There has been extensive research on differentiation of functioning white fat cells which are responsible for synthesizing, storing, and releasing lipids, and brown fat cells which burn off adenosine triphosphates (ATP, see following section for detail.) For both white and brown fat cells, the transcription factor

FoxO1, plays a key role. FoxO1+/- mice with smaller, "healthier" fat cells were protected from T2D upon administration of a HFD, which may have suppressed (PPAR)-γ and its accessory transcriptional elements [90]. They demonstrated that a greater-negative side of FoxO1 augments ATP expenditure in BAT, suggesting inhibition of FoxO1 in white or brown fat may have a therapeutic effect on T2D and/or obesity by maintaining energy homeostasis. Further, Zou et al. demonstrated that FoxO1 is unable to phosphorylate adipocytes, which is inversely related to its function, providing a tide-like, composite sequence throughout adipogenesis based on the timing of FoxO1 blockade with a specific inhibitor, AS1842856, which can prevent further transcriptional events [90]. Consistent with this study, genes from our RNAseq data involved in the FoxO signaling pathway, such as PCK2, were upregulated in MFGR compared to MC. Thus, investigation of PCK2 and the rest of the FoxO signaling pathway gene list in Fig. 14 provide new areas for research.

There were no significantly enriched pathways in the FFGR_FC comparison, which is most likely due to the small size of the FFGR_FC DESEQ2 dataset (P-adj<0.05, Table 12, Fig. 15). The most significantly enriched pathway is the estrogen signaling pathway, most likely because of the immense biological role that estrogen plays in female development. HSPA6, which is significantly dysregulated in both MFGR_MC and FFGR_FC comparisons has a prominent role in the estrogen signaling pathway. Sex hormones play a key role in fat distribution and adipocyte differentiation (see previous section for details). For example, estrogens and estrogen receptors control numerous aspects of lipid metabolism and glucose homeostasis. Disturbances in utero to these pathways increase risk of cardiovascular disorders and metabolic syndrome in females. During menopause, the absence of estrogen is an obvious factor in the onset of heart disease characterized by lipid content fluctuations and excess abdominal fat accumulation. However, the exact relationship between estrogen levels and higher obesity in women during menopause is not clear. A large amount of research has examined the effect of estrogen-like compounds and endocrine disruptors in adiposity, suggesting a decrease in estrogen secretion correlates with obesity in females [91]. While these pathways are not statistically significant to the FFGR_FC comparison, the lack of statistical significance suggests there are fewer genetic adaptations to FGR in females than males. Perhaps this lack of differential gene expression can help explain the lack of protection against T2D and obesity in the FFGR group.

Fig. 16-18 begins to paint an overall picture of prevalent genes and protein interactions that are differentially expressed in FGR vs control males and females, providing lists of FGR-mediated obesity related gene targets and their relationships. Following qPCR and Western Blot validation, our functional analysis describes targets for *in vitro* and *in vivo* mouse KO and knock-in studies. Unlike the gene targets for KO studies investigating adipose tissue programming in males vs females, these gene targets are concerned with the how FGR may increase susceptibility to obesity respective of sex.

Cis-regulatory and trans-acting factors appear to lead to the dysregulation of several genes belonging to the canonical and functional pathways mentioned in the current study (Fig. 19). A Zinc-like finger, ZNF384, was identified as a binding site in the promoter region of the top dysregulated genes from all group comparisons. This suggests FGR-mediated programing of ZNF384 expression leads to decreased adipogenesis in males and increased adipogenesis in females, along with increased fat storing capacity in FGR compared to control males and females. Further experiments are necessary, however, to establish the role of ZNF384 in regulating pathways such as FoxO and PI3/AKT, and their role in FGR-mediated postnatal catch-up growth. The present report provides strong rationale for such studies [67].

A DNA-binding domain Forkhead box protein K1 (FOXK1) was identified as a binding site in the promoter regions from our MFGR_MC comparison (Fig. 21). FOXK1 is an inhibitor of JNK-associated Leucine Zipper Protein (JLP). Considering the FoxO signaling pathway is prevalent in the MFGR, this provides a strong rationale for investigation of JLP as a Docking platform in the FoxO signaling pathway [92].

A transcriptional repressor RE1-Silencing Transcription Factor [93] was identified as a binding site in the promoter regions from our FFGR_FC comparison (Fig. 22). REST is an inhibitor neural genes and non-neuronal cells. REST signaling is associated with cell death and cell fate determination [94]. Given the multipotency of preadipocytes, this provides a strong rationale for investigating the role of REST in adipogenesis focusing on its role in beiging of brown adipocytes. These two motifs, FOXK1 and REST, might reveal important dysregulated pathways that occur as a result of FGR.

Due to changes in perirenal fat depots in response to FGR, a number of studies have investigated brown adipocyte size and morphology differences, paying special interest to lipid accumulation. It has repeatedly been shown that FGR is associated with increased lipogenesis, decreased lipolysis, and greater serum and liver triglyceride (TG) content [57] [95] [96]. Recently, it has been shown that reduced meal frequency and every other day fasting (EODF) can decrease susceptibility to HFD-induced obesity by decreasing serum triglyceride, liver and adipocyte lipid content, and liposaccharide concentrations in mice and pigs [97]. In some cases, EODF has restored BAT and liver lipid content in HFD-induced mice to control levels [41]. Therefore, diet restriction may potentially decrease risk of obesity and may serve as a therapeutic strategy for FGR neonates.

FGR babies are prone to central redistribution of adipose tissue which may persist postnatally and lead to increased insulin resistance. Along with their role in sex differences, adipocytokines from VAT play an important role is modulating metabolism in FGR. Lower expression of leptin, adiponectin, and higher expression of ghrelin are associated with FGR babies so these are considered possible indicators of long-term indicators of obesity [98]. This makes sense considering leptin is a satiety signal, ghrelin is a hunger signal, and adiponectin regulates blood glucose levels and breaks down fatty acids [98]. Furthermore, expression of leptin 24 hours following birth is necessary for proper adipogenesis. Dysregulation of leptin following birth is attributed to overexpression of PPAR-y, which may be the reason the present study observed increased rates of adipogenesis and lipid accumulation in FGR females compared to controls. There are a lot of ongoing research investigating the roles of these hormones in obesity and diabetes and yet the exact endocrinology dysregulation that occurs in these disorders is not well-known.

CHAPTER 3

The Brown Adipocyte

Recent evidence has shown that along with endocrine dysregulation, WAT to BAT composition following birth also plays a large role in susceptibility to obesity. Specifically, the overaccumulation of WAT and a reduction in BAT associated with FGR and rapid catch up growth increases the risk for obesity in adulthood. This is partially due to the main role of WAT in energy storage in the form of triacylglycerol as a long-term fuel supply [99]. Large unilocular lipid droplets found in white adipocytes allow for greater lipid storage in contrast to smaller, multilocular lipid droplets found in brown adipocytes [100]. During starvation these fuel reserves are accessed and free fatty acids are mobilized via oxidative phosphorylation and broken down into ATP.

Unlike WAT, BAT does not release ATP via electron transport chain [101] coupling with ADP phosphorylation. Instead, BAT releases energy in the form of heat and is essential to prevent postnatal hypothermia through non-shivering thermogenesis [102]. Briefly, this pathway is activated by a cold stimulus, causing the release of norepinephrine (NE) into the bloodstream. Then, NE binds to the beta-adrenergic G-protein receptor in mature brown adipocytes and once activated, the G-protein activates adenylate cyclase, which converts ATP generated by oxidative phosphorylation into cAMP. Then, cAMP activates Protein Kinase A (PKA) which communicates with HSL to break down triglycerides into NEFAS in adipocytes, which are mobilized to target cells for beta oxidation. Once free fatty acids enter the mitochondria of target cells, they cross the mitochondrial inner membrane space by palmitoyl carnitine transferase 1 (CPT1) and bind to UCP-1 and/or enter the mitochondrial matrix by CPT2. Upon binding to UCP-1 receptors on the mitochondrial inner membrane, UCP-1 leaks protons from the intermembrane space into the mitochondrial matrix. Increases in proton conductance dissipates the mitochondrial electrochemical gradient and the proton motive force generates heat rather than ATP during oxidative phosphorylation, which burns fat instead of storing energy. Not only does this release of energy in the form of heat burn fat but uncoupling provides larger quantities of H+ for fatty-acid beta oxidation than oxidative phosphorylation. This increases beta oxidation by allowing for low substrate beta oxidation with a low rate of ATP production because the electron carriers (NAD and FAD) are supplied with more H+ than during energy conserving rates. Thus, larger amounts of BAT and BeAT increase the rate at which fatty acids are broken down into acetyl and acyl-CoAs, the building blocks for ketone bodies providing more usable energy. To note, the transition from glucose utilization to ketone bodies for energy has been shown to burn more fat in fed and fasted states in mice [103]. Furthermore, fasting and refeeding cycles are associated with increased browning of white adipocytes and enhanced glucose storage and utilization in the fed state, suggesting its relevance in T2D and obesity [103].

In order to better understand the mechanisms that differentiate perirenal BAT and WAT adipose tissue remodeling, it is necessary to examine isolated mature white, brown, and beige adipocytes. Beige adipocytes are multipotent of preadipocytes. In theory, preadipocytes destined to be white adipocytes can be differentiated into UCP-1 expressing beige/brown adipocytes. This presents a novel area of research, the investigation of differentiation rates of mature brown adipocytes in HFD, calorie restricted (CR), FGR, obese and diabetic individuals. Differentiation of brown adipocytes is the maturation of preadipocytes into UCP-1 expressing mature adipocytes which release energy in the form of heat (non-shivering thermogenesis). UCP-1 is a specific molecular marker found in the inner membrane of mature brown adipocytes. UCP-1 expression in BAT is particularly prevalent days 1-6 postnatally in Eutherians (placenta mammals) where neonates must stay warm, especially if born in colder months.

The majority of preadipocytes in BAT begin differentiating shortly after birth. If nutrients are not scarce postnatally, the rate of preadipocyte differentiation to adipocytes is similar in IUGR and normal neonates. This mismatch of total body weight and amount of fat depots creates an obstacle, because FGR babies are born without a healthy proportion of lean-to fat body mass. This results in infants with higher levels of abdominal fat and increased centralized fat distribution with resultant obese phenotype [104].

Excessive conversion of preadipocytes to mature adipocytes is a chief contributor to obesity in humans. In order for normal BAT development, regulation of adipogenesis is crucial and this process is highly regulated by gene expression. Of importance, FGR groups in the present study showed increased differentiation rates of brown adipocytes than controls and the MFGR group exhibited decreased differentiation rates compared to FFGR. Since preadipocytes act as continuous renewable sources of adipocytes, they control the number of mature adipocytes and thus, the capacity for fat storage [105]. Therefore, examining differential gene expression between preadipocytes and mature adipocytes in male and female FGR and controls remains a potential future study.

Our results indicate a nuanced sexual dimorphism where FGR appears to affect BAT proliferation, morphology, and lipid deposition in females differently than males. In particular, it appears MFGR confer a fitness advantage over women by increasing lipolysis rates in response to placental insufficiency, protecting them from adulthood obesity. Differential gene expression in male and female perirenal adipose gene expression plays a prominent role in these sex differences. Genes that are significantly differentially expressed in perirenal adipose tissue from male and females in literature include: ACTC1, SOX2, insulin, CEBP-α, CREBBP, ADIRF-1, NDUFA12, NDUFB3, PPAR-γ, FRMD4A, PRDM16, Transforming Growth Factor-Beta (TGFß), Adiponectin (Adipoq), Leptin (LEP), Glycerol-3-phosphate Dehydrogenase-2 (GDPD2), Fatty-Acid Synthase (FASN), and Solute Carrier Family 2 Member 1 (GLUT4) [40].

Some limitations of our study include lacking validation of gene expression results by qPCR or Western Blot, isolating RNA directly from adipose tissue rather than mature brown adipocytes, and lacking *in vivo* experiments. Thus, future studies should include the investigation of the epigenetic pathways involved in adipogenesis and how specific biomarkers are dysregulated under FGR using a multi-omics approach towards understanding adiposity. This would involve adipose-derived stem cell isolations and subsequent preadipocyte differentiation into mature adipocytes prior to RNA isolation for Bisulfite Sequencing (methylation patterns), RT-PCR, and Western Blot Analysis.

Figures

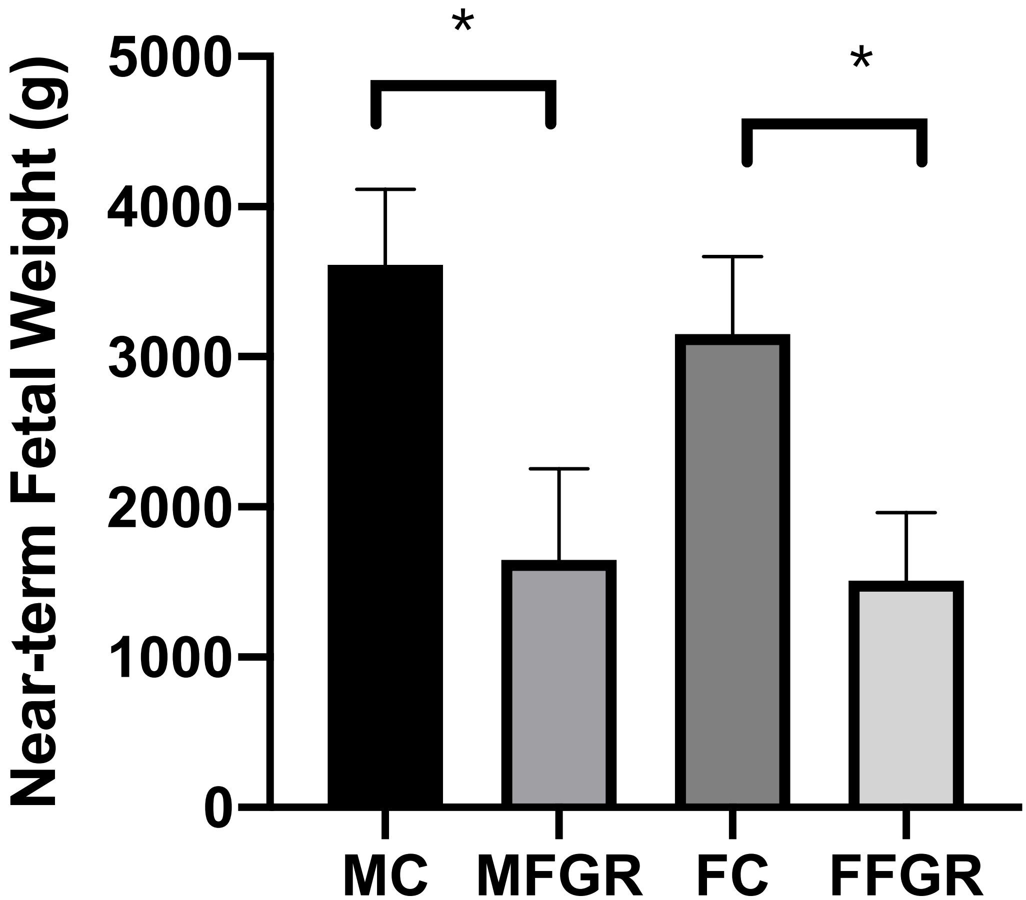

Fig 1: Near-term weights from Male Control, Male Growth-Restricted, Female Control, and Female Growth-Restricted fetal lambs**.** N = 16 each group. * Denotes P-Value. < 0.05 in a two-way ANOVA comparison of means for Sex and FGR differences.

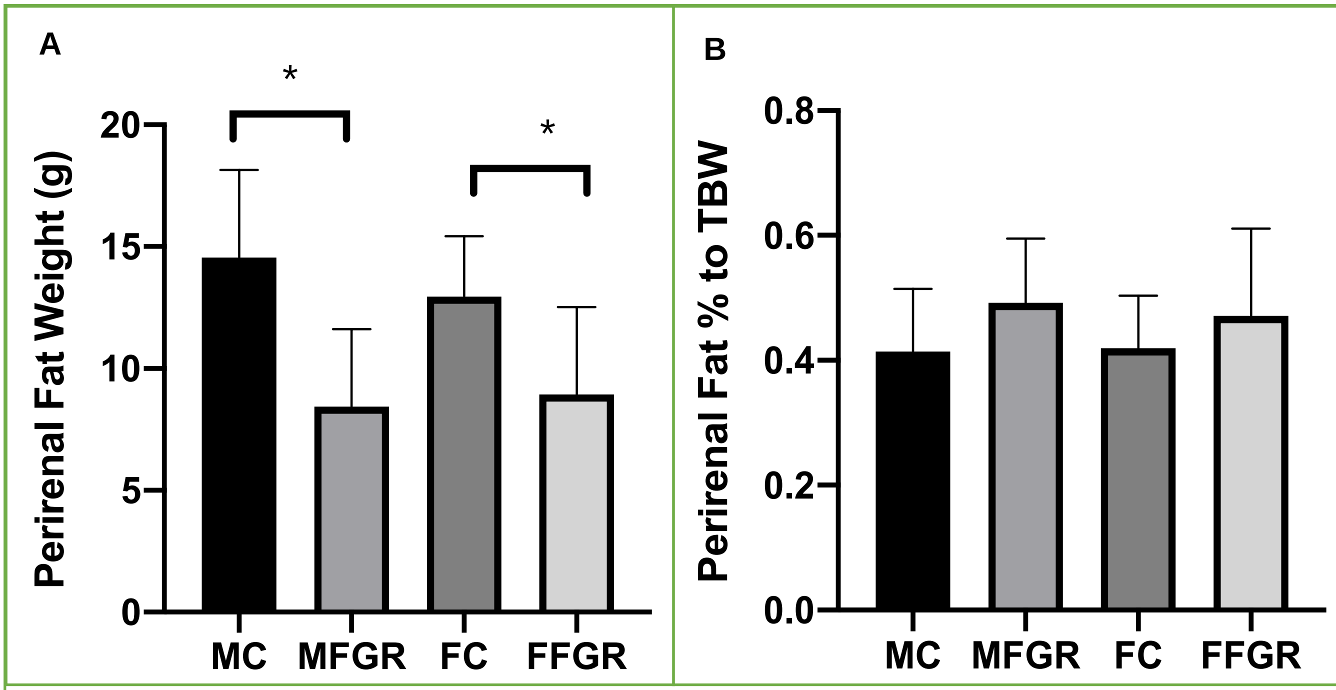

Fig 2A: Perirenal fat weights of near-term Male Control, Male Growth-Restricted, Female Control, and Female Growth-Restricted fetal lambs**.** N = 16 each group. * Denotes P-Value. < 0.05 where a Two-Way ANOVA comparison of means for Sex and FGR differences. **B:** Perirenal fat represented as a % of Total Body Weight (TBW).

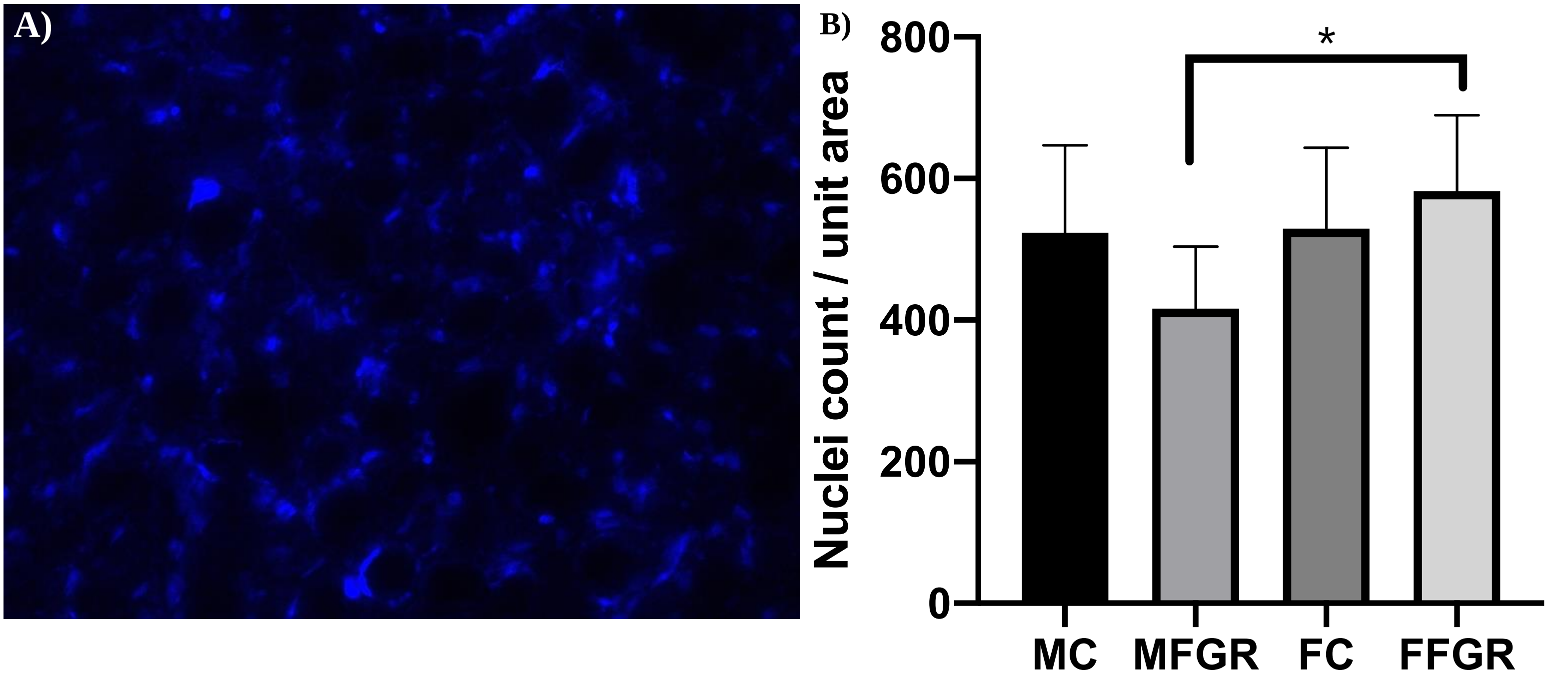

3A: DAPI stained images of adipocytes taken on a Leica fluorescent microscope from Male Control, Male Fetal Growth-Restricted, Female Control and Female Growth-Restricted fetal lambs. Nuclei were pseudocolored blue on ImageJ (400x magnification). **Fig 3B**: Cell density was determined by counting DAPI stained Nuclei. N = 4 each group. *Denotes P-Value < 0.05 in a Two-Test ANOVA comparison of means for Sex and FGR differences.

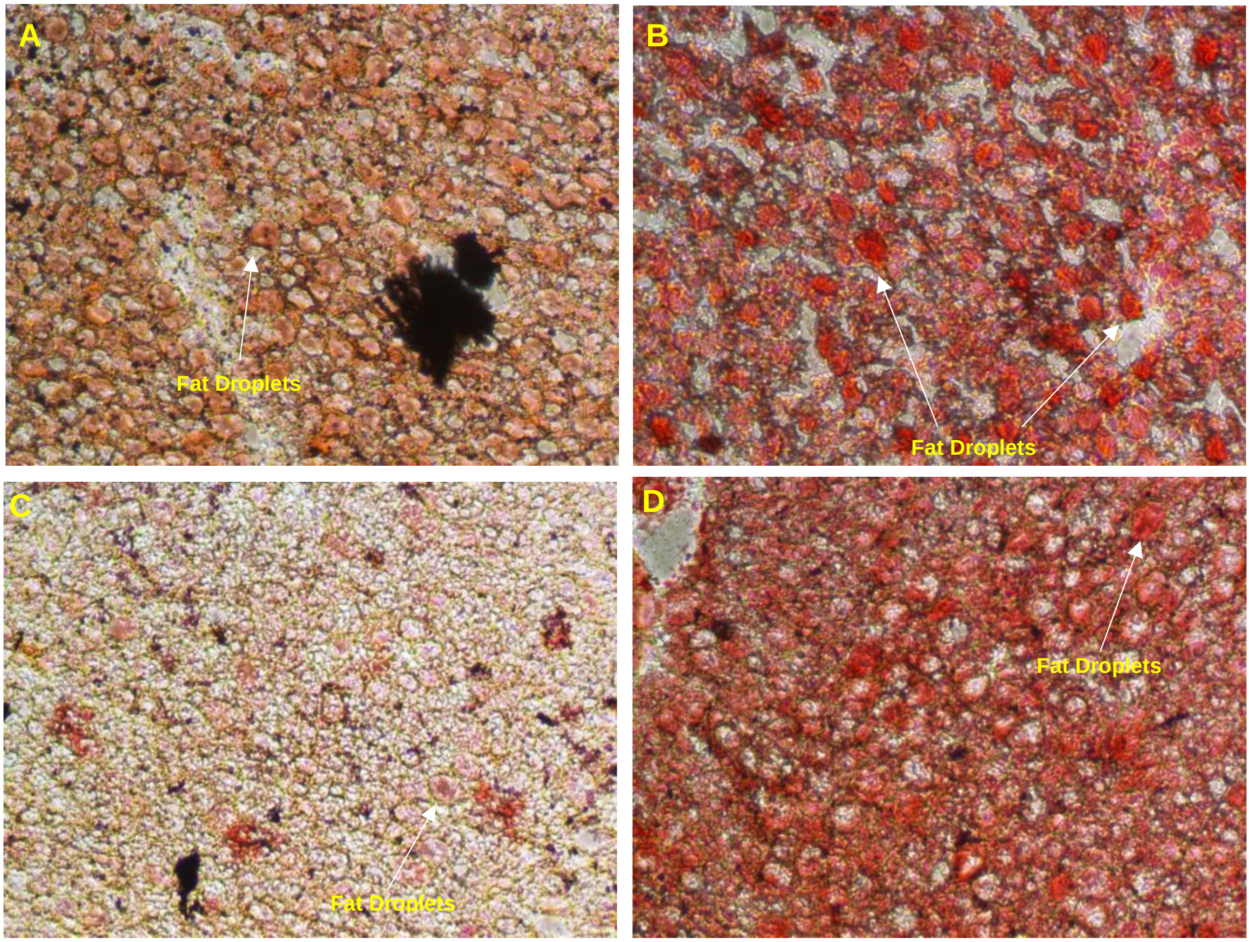

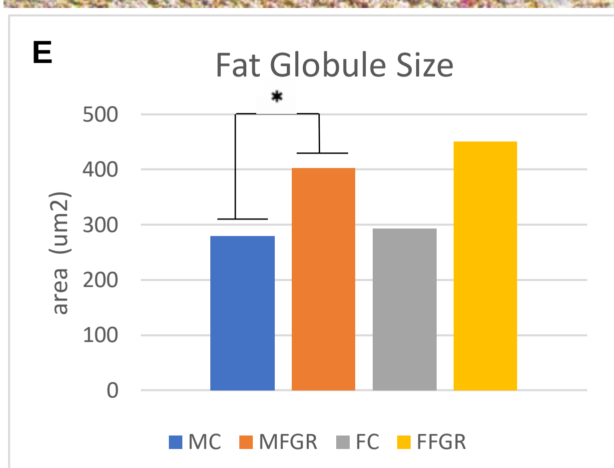

Fig 4: Demonstrates histology of perirenal fat and fat globule size by Oil Red O staining of adipocytes. (A) Perirenal fat from a Male Control fetal lamb. (B) Perirenal fat from a Male Growth-Restricted fetal lamb. (C) Perirenal fat from a Female Control fetal lamb. (D) Perirenal fat from Female Growth Restricted fetal lambs. (E) Bar graph of average globule area for each group. N = 4 each group. * Denotes P- adj. < 0.05.

4F: A Bonferroni correction for multiple comparison T-test for significant differences in average globule size between the four two-way comparisons: FC vs. FFGR, FC vs. MC, FC vs. MFGR, FFGR vs. MC, FFGR vs. MFGR, and MC vs. MFGR (P-adj. <0.05, right).

group1	group2	n1	n2	p	p.adj	p.adj.
<chr>	<chr>	<int>	<int>	<dbl>	<dbl>	<chr>
FC	FFGR	18	12	0.161	0.966	ns
FC	MC	18	15	0.114	0.684	ns
FC	MFGR	18	15	0.133	0.798	ns
FFGR	MC	12	15	0.016	0.097	ns
FFGR	MFGR	12	15	0.749	1	ns
MC	MFGR	15	15	0.002	0.011	*

F

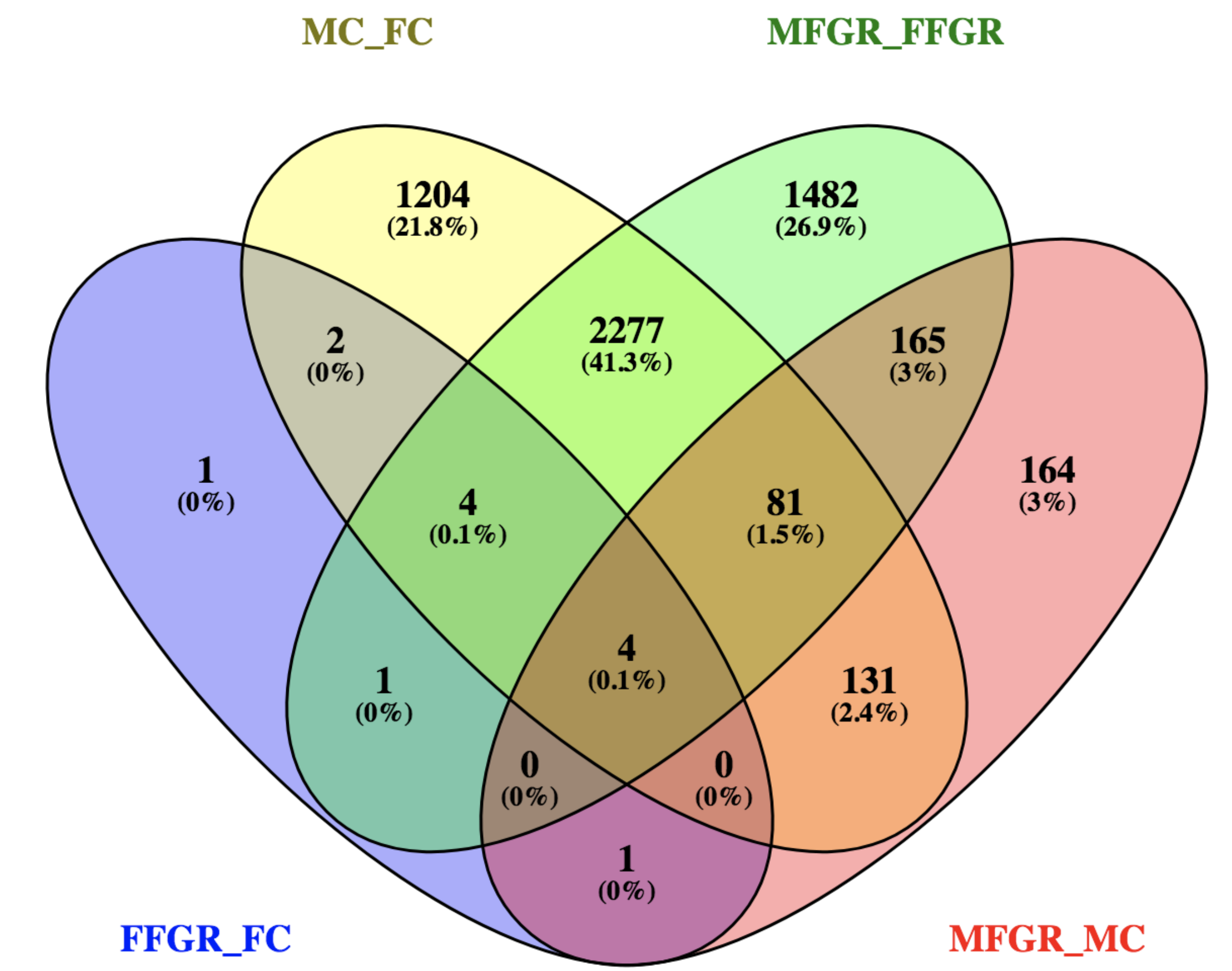

Fig 5: Venn diagram demonstrating common transcripts that were significantly different between all four group comparisons according to log2FoldChange values transformed from Raw Counts: Male Control vs. Female Control, Male Growth-Restricted vs. Female Growth-Restricted, Female Growth Restricted vs Female Control, and Male Growth-Restricted vs. Male Control fetal lamb perirenal fat (P-adj. values < 0.05). N = 4 in each group.

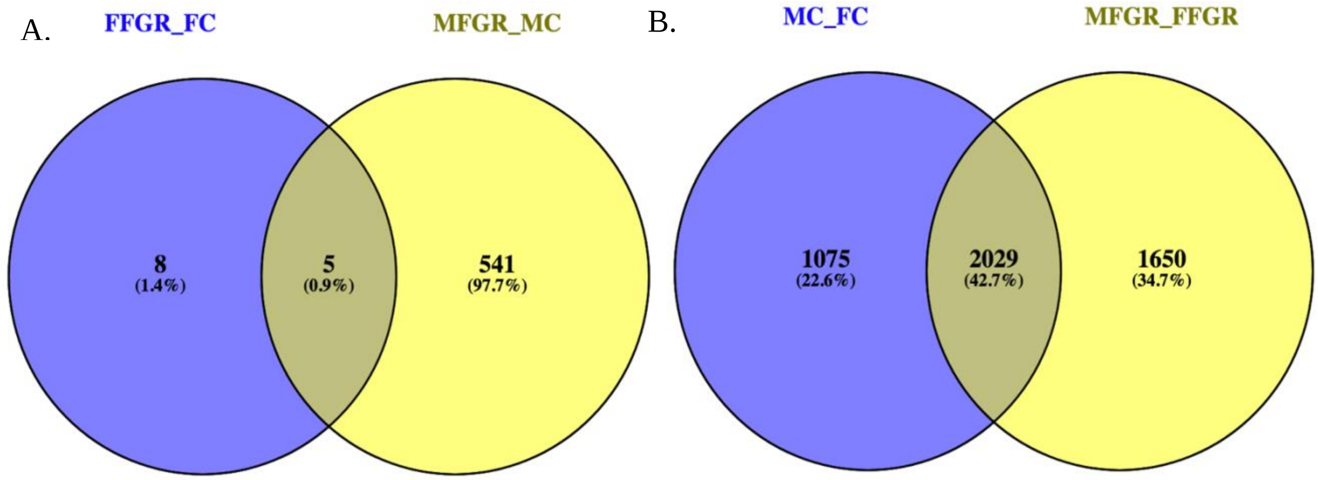

Fig. 6: Venn diagram comparing shared significantly different transcripts (A) between Fetal Growth-Restricted Control Male and Female fetal lamb perirenal fat and between (B) male and female fetal lamb perirenal fat from control and FGR groups (P-adj <0.05). N=4 in each group.

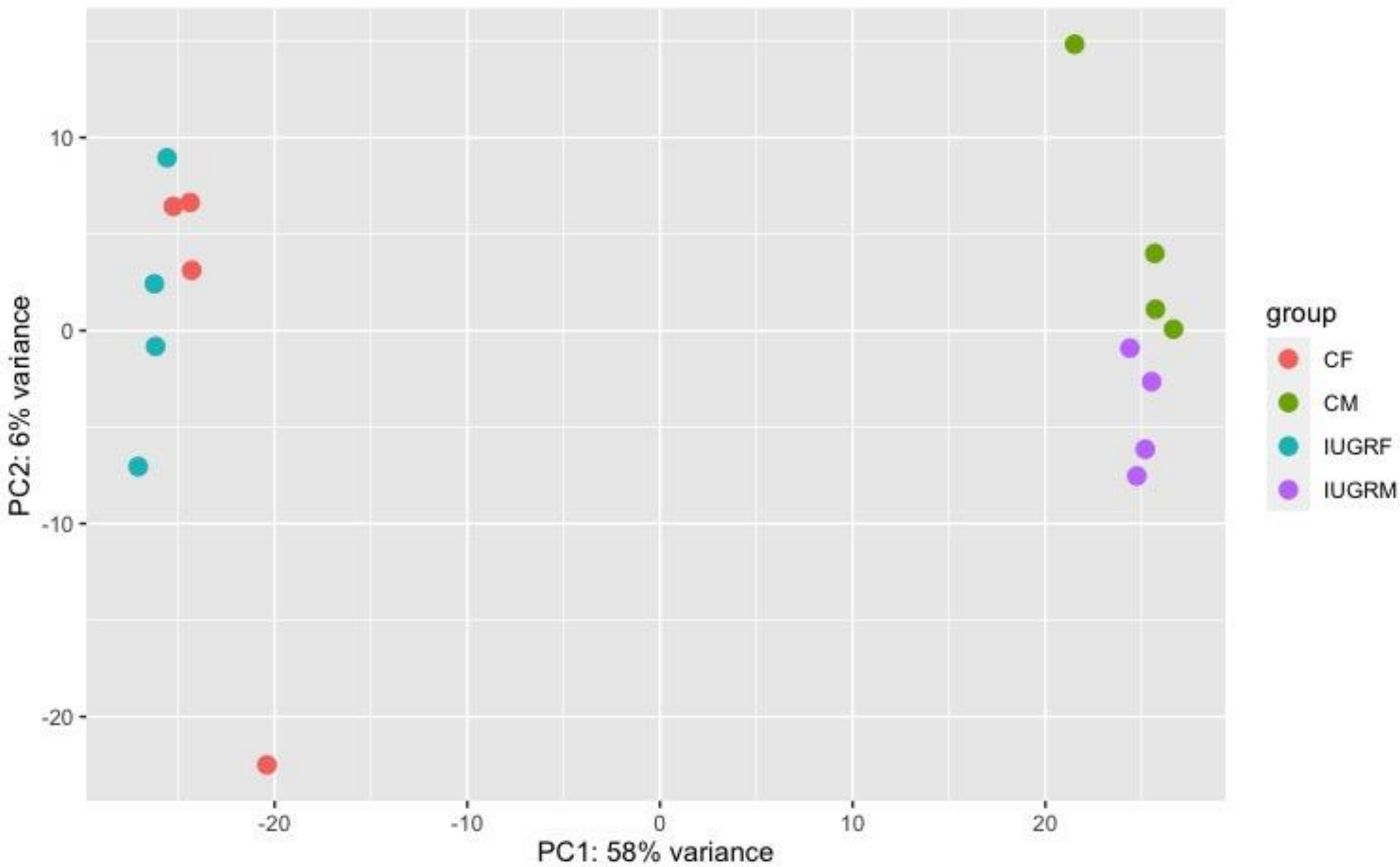

Fig. 7: Principal Component Analysis from DESeq2 dataset showing similarity between log2FoldChange Values of Raw Counts in Male Control, Male Growth-Restricted, Female Control, and Female Growth-Restricted fetal lamb perirenal fat based on significantly different transcripts between groups (P-adj <0.05). N=4 in each group.

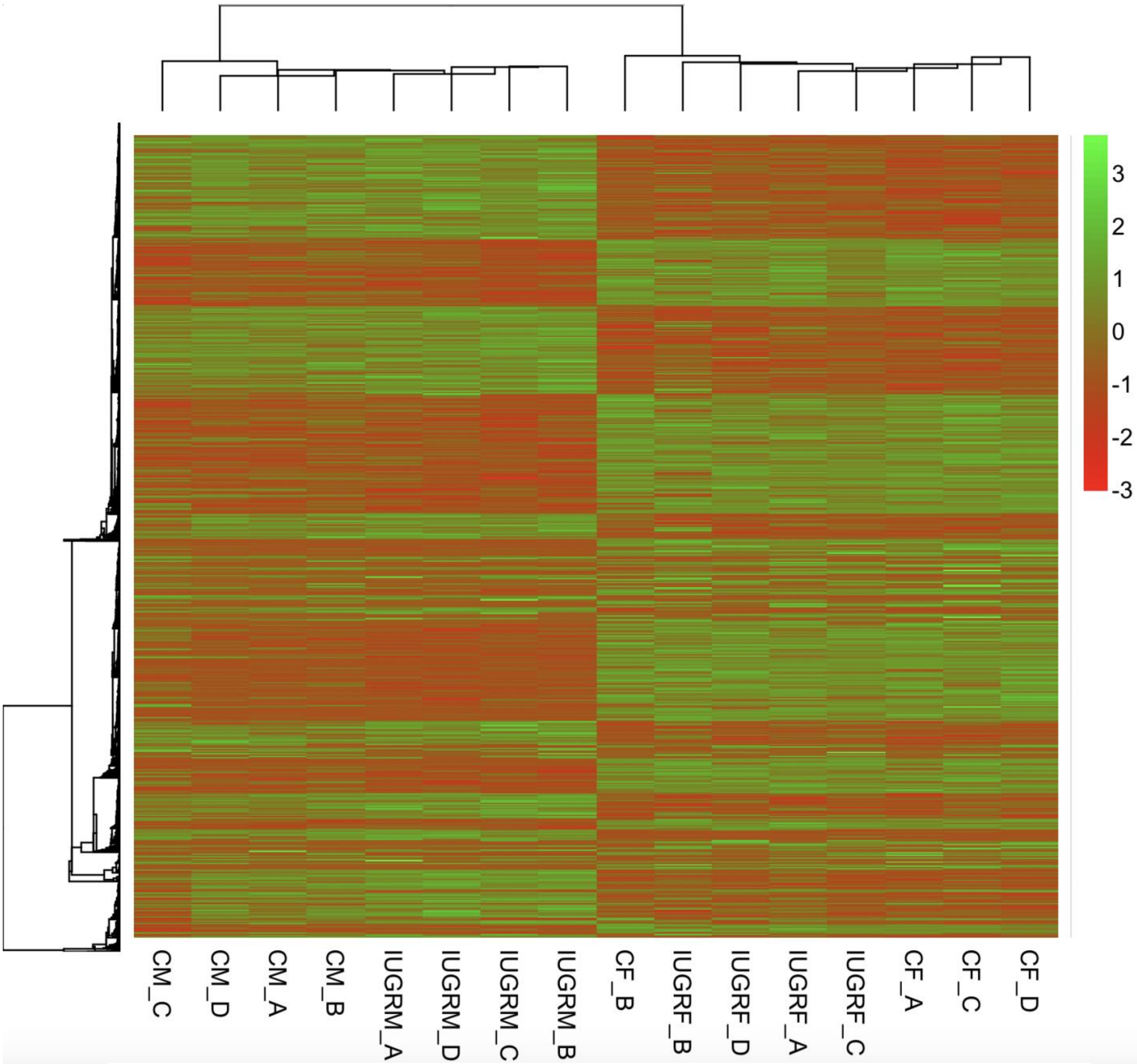

Fig. 8: A Heatmap representing between and within group differences according to significantly different transcripts (P-adj. < 0.05). The color denotes log2FC values of Raw Counts transformed into Z-scores, where green=upregulated and red=downregulated (-3<Z-Score<3). Dendrograms on the x-axis and y-axis represent hierarchical clustering of samples and transcripts, respectively. N=4 in each group.

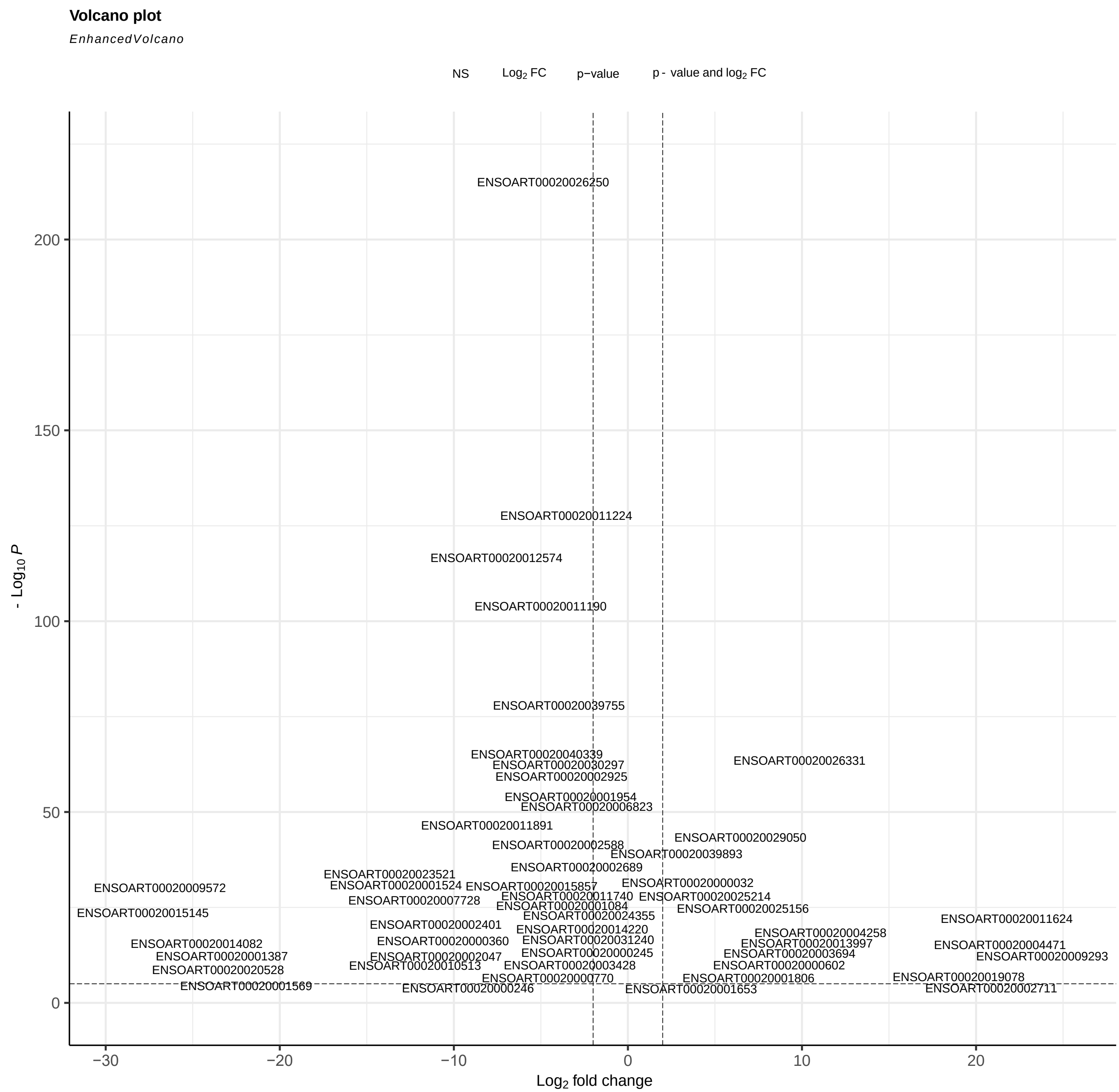

Fig. 9: Volcano plot representing significantly different transcripts in perirenal fat from fetal lambs of all four groups according to log2FoldChange values of Raw Counts and P-adj. values (log2FC>|1.5|, P-adj<10e^{-10}). Red dots represent transcripts that meet both cut-offs, green dots meet the comparison for log2FC, blue dots meet the cut-off for P-adj., and grey dots meet neither cutoff. log2FC values were not shrunk as they were in the remaining volcano plots because the lfcshrink command in R-studio requires no more than two groups in the comparison. This volcano plot includes all four groups.

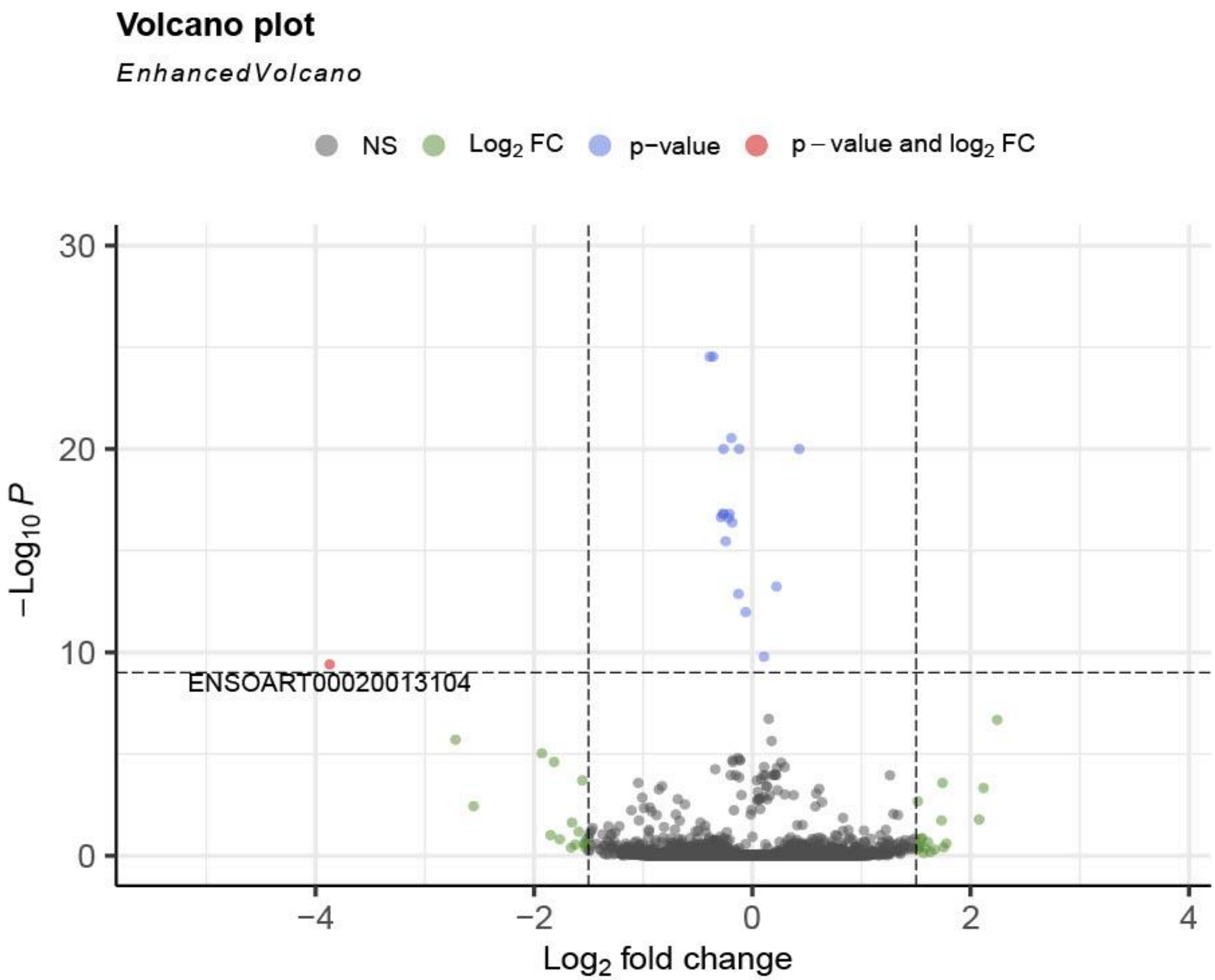

Fig. 10: Volcano plot representing significantly different transcripts in perirenal fat from Male Growth-Restricted compared to Male Control fetal lamb perirenal fat according to log2FoldChange values of Raw Counts and P-adj. values (P-adj<10e^{-10}, log2FC>|1.5|). Values were shrunk using lfcshrink command from ggplot2 in R-studio. Log2FC was calculated using MFGR log2FC as the numerator and MC log2FC as the denominator. N=4 in each group.

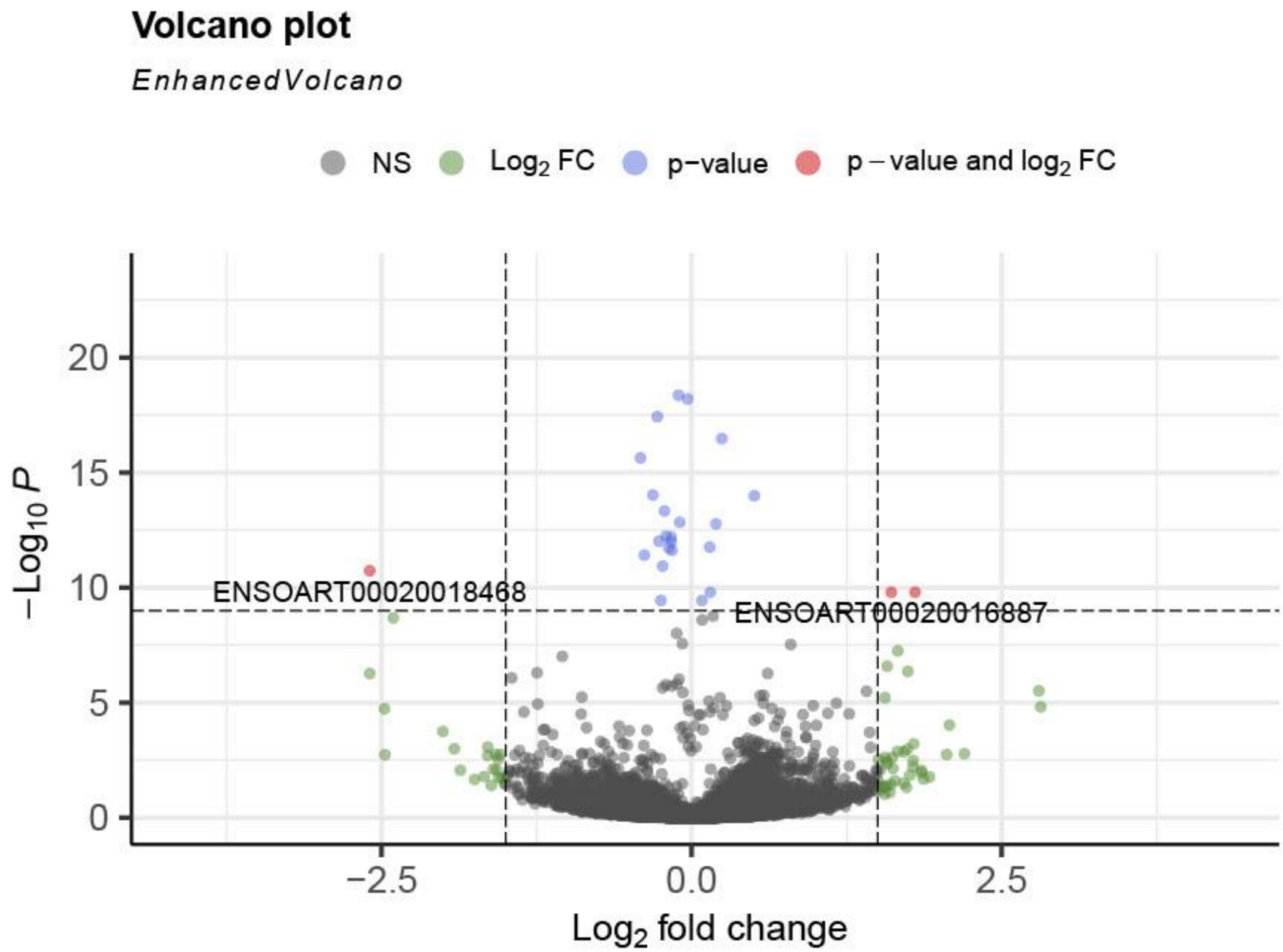

Fig. 11: Volcano plot representing significantly different transcripts in perirenal fat from Female Growth-Restricted compared to Female Control fetal lambs according to log2FoldChange values of Raw Counts and P-adj. values (P-adj<10e^{-10}, log2FC>|1.5|). Values were shrunk using lfcshrink command from ggplot2 in R-studio. Log2FC was calculated using FFGR log2FC as the numerator and FC log2FC as the denominator. N=4 in each group.

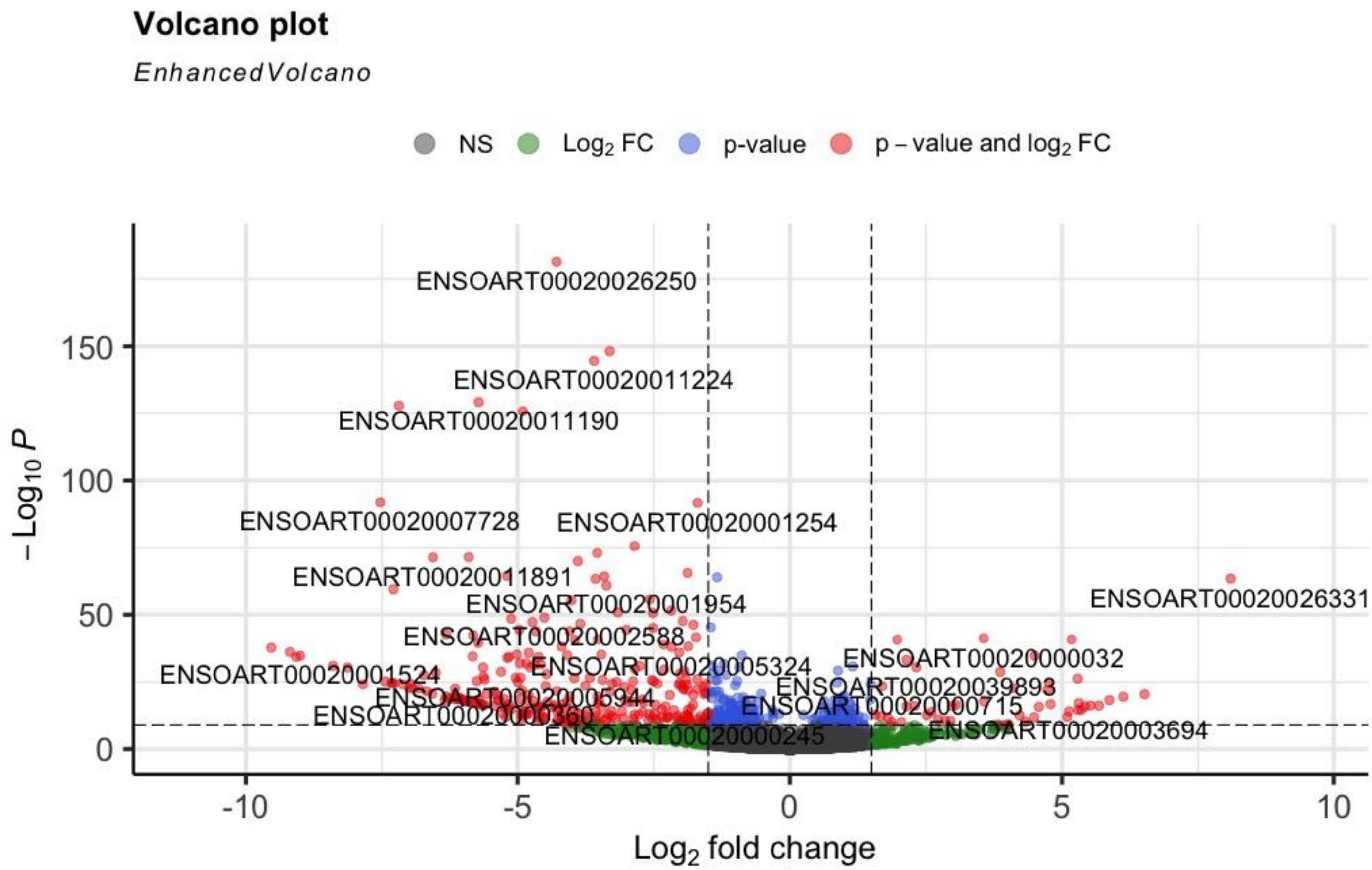

Fig. 12: Volcano plot representing significantly different transcripts in perirenal fat from Male Control compared to Female Control according to log2FoldChange values of Raw Counts and P-adj. values (P-adj<10e^{-10}, log2FC>|1.5|). Values were shrunk using the lfcshrink command from ggplot2 in R-studio. Log2FC was calculated using MC log2FC as the numerator and FC as the denominator. N=4 in each group.

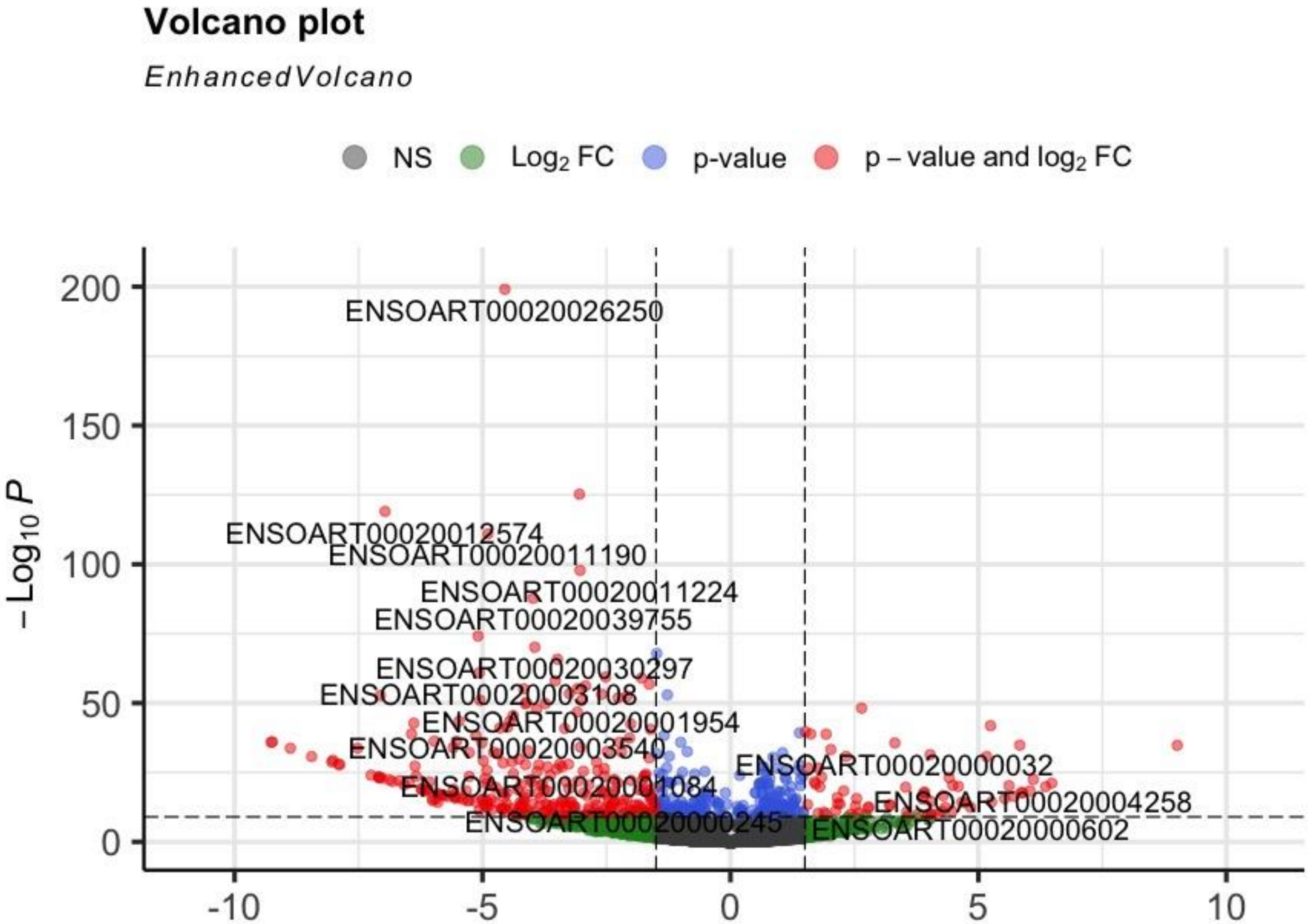

Fig. 13: Volcano plot representing significantly different transcripts in perirenal fat from Male Growth-Restricted compared to Female Growth-Restricted fetal lambs according to log2FoldChange values of Raw Counts and P-adj. values (P-adj<$10e^{-10}$, log2FC>|1.5|). Values were shrunk using lfcshrink command from ggplot2 in R-studio. Log2FC is calculated using MFGR log2FC as the numerator and FFGR log2FC as the denominator. N=4 in each group.

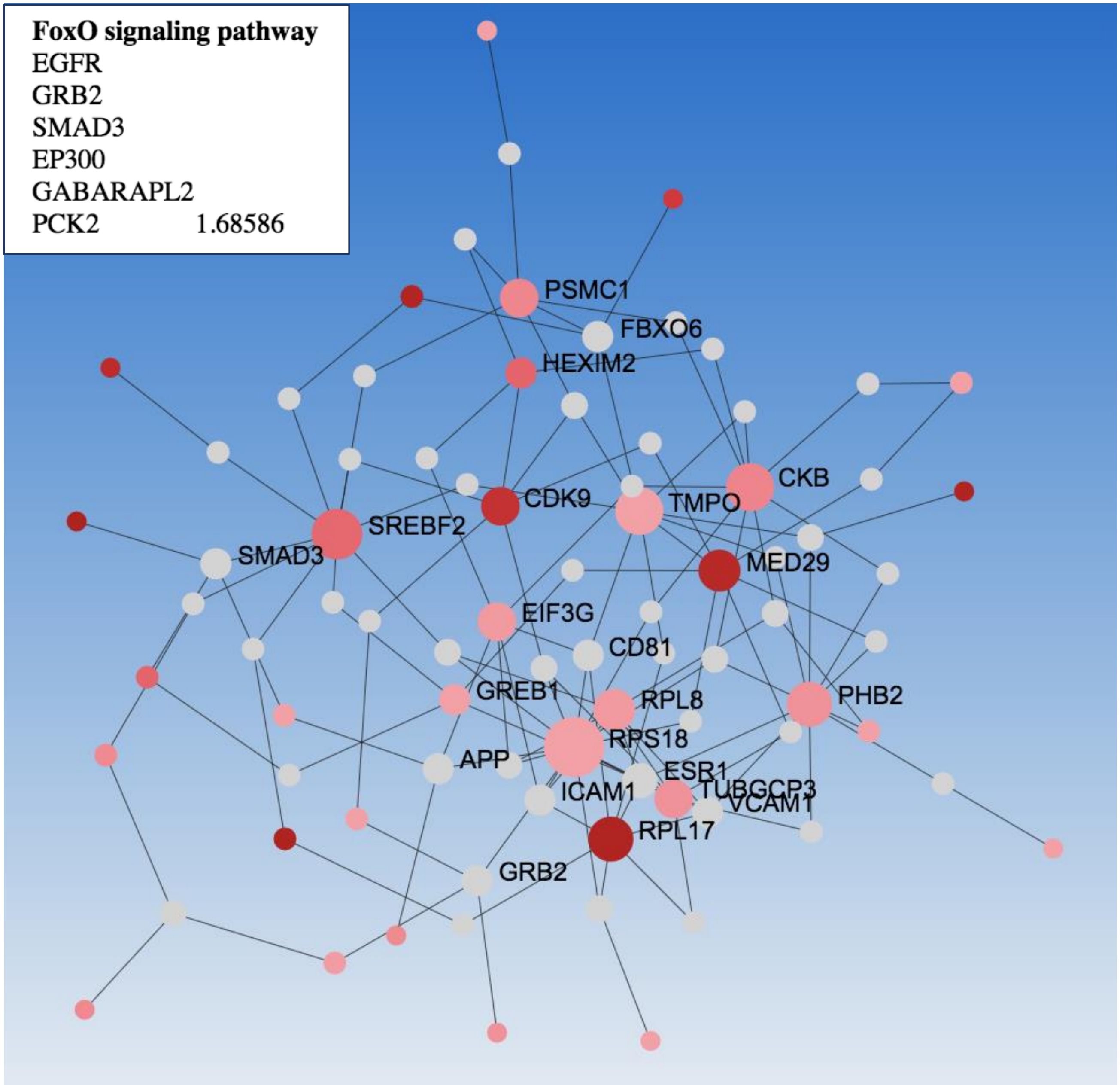

Fig. 14: Minimum Gene Network of the 50 most significantly dysregulated transcripts in the Male Growth-Restricted vs. Male Control comparison of perirenal fat from fetal lambs ranked by P-adj. values (greatest P-adj =0.00062) showing adipose tissue specific Protein-Protein-interactions (PPI). Sheep transcripts were converted to human orthologs prior to running Gene Analyst and are represented as proteins in the Network. The size of the circle represents betweenness, the color denotes expression where red is upregulated and green is downregulated, and edges between nodes indicate relationships between proteins. The most significant KEGG pathway is in the top left of the figure.

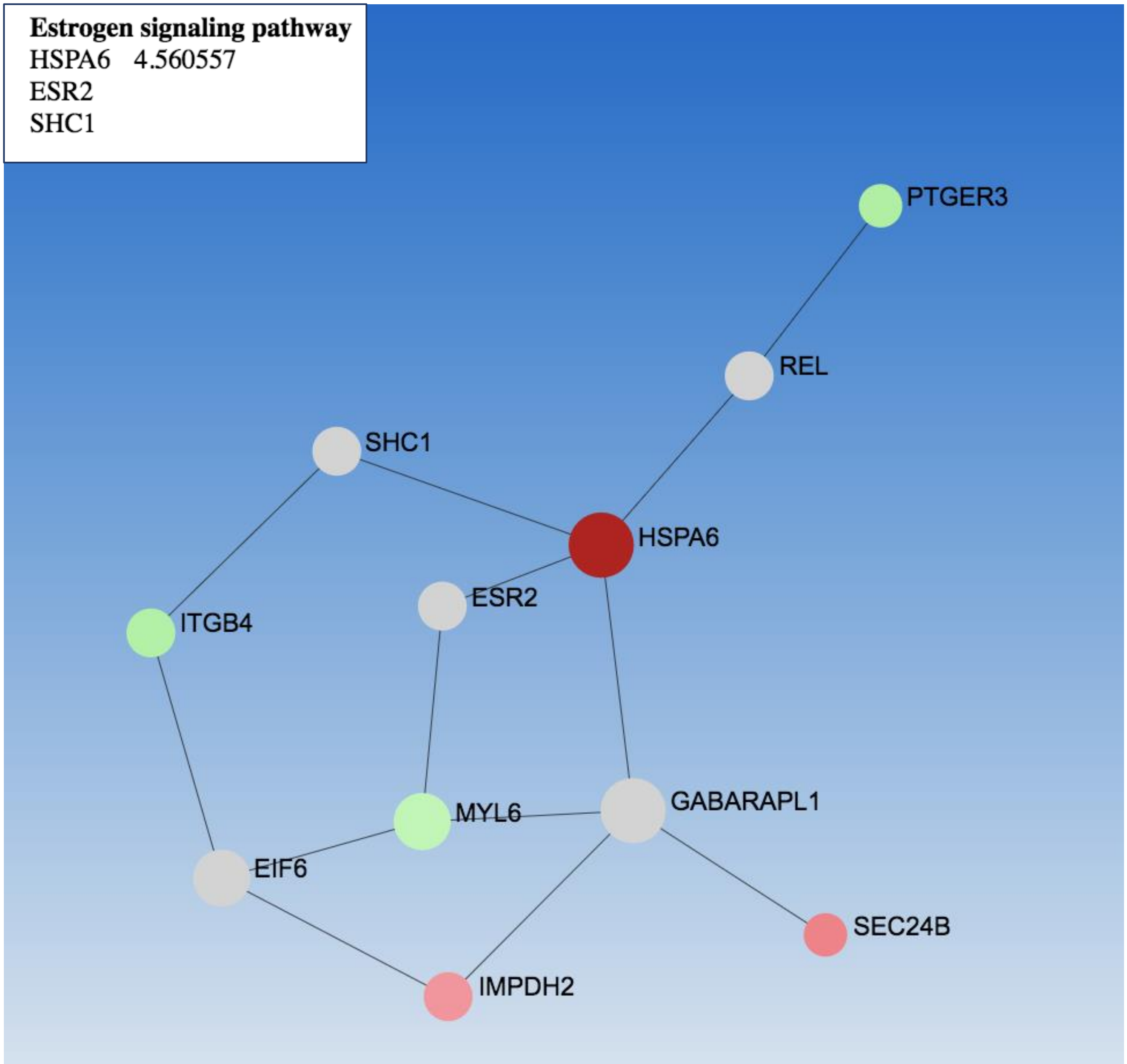

Fig. 15: Minimum Gene Network of the 13 most significantly dysregulated transcripts in Female Growth-Restricted vs Female Control comparison of perirenal fat from fetal lambs ranked by P-adj. values (greatest P-adj =0.032) showing adipose tissue specific PPI. There were 13 signficantly different transcripts in the gene list so this network comprises the entire DESeq2 data set for the FFGR vs. FC comparison. Sheep transcripts were converted to human orthologs and represented as proteins in the Network. The size of the circle represents betweenness, the color denotes expression where red is upregulated and green is downregulated, and the edges indicate relationships between proteins. The most significant KEGG pathway is in the top left.

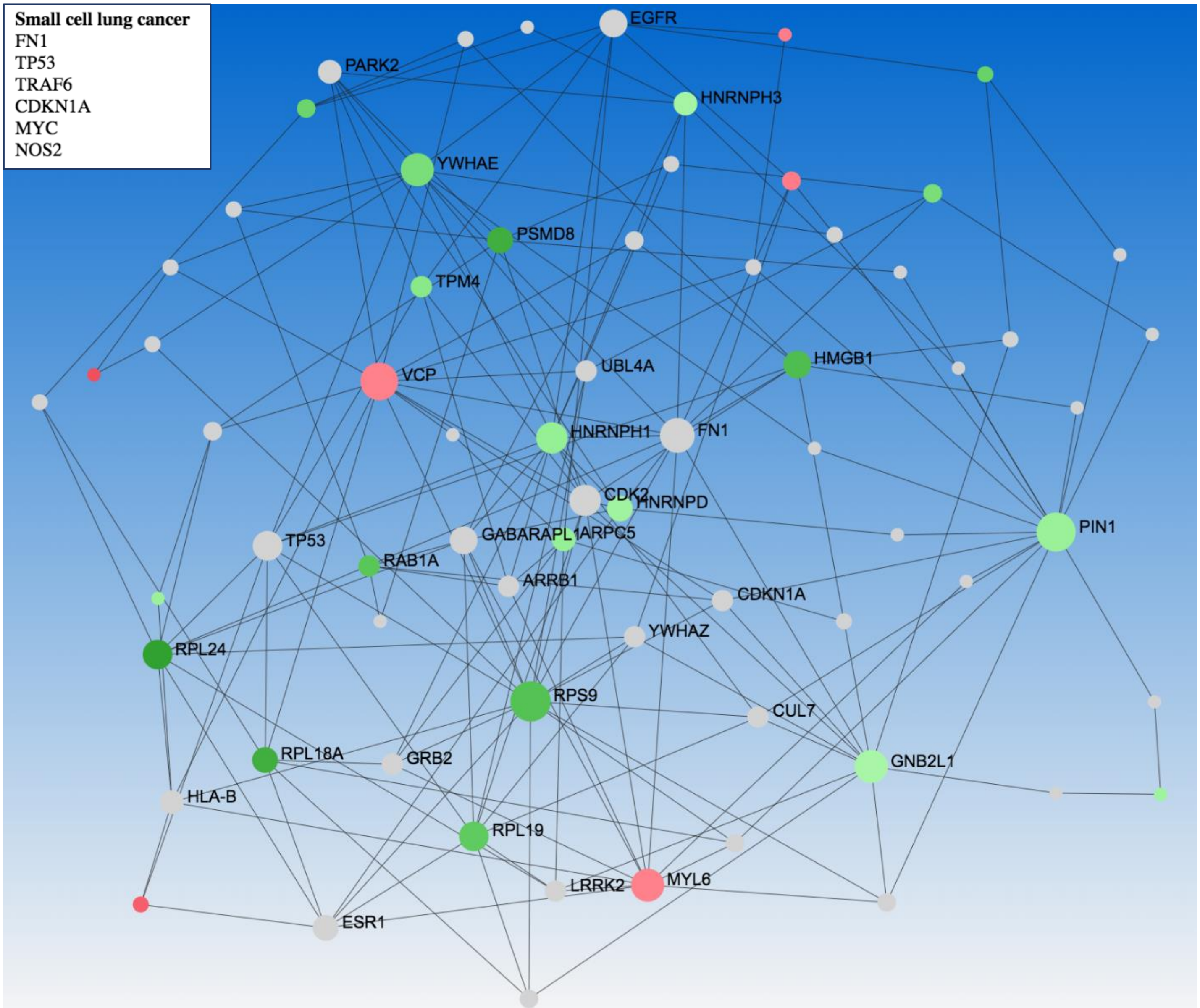

Fig. 16: Minimum Gene Network of the 50 most significantly dysregulated transcripts in the Male Control vs Female Control comparison of fetal lamb perirenal fat ranked by P-adj. values (greatest P-adj =5.8e^{-30}) showing adipose tissue specific PPI. Sheep transcripts were converted to human orthologs and represented as proteins. The size of the circle represents betweenness, the color denotes expression where red is upregulated and green is downregulated, and the edges indicate relationships between proteins. The most significant KEGG pathway is in the top left.

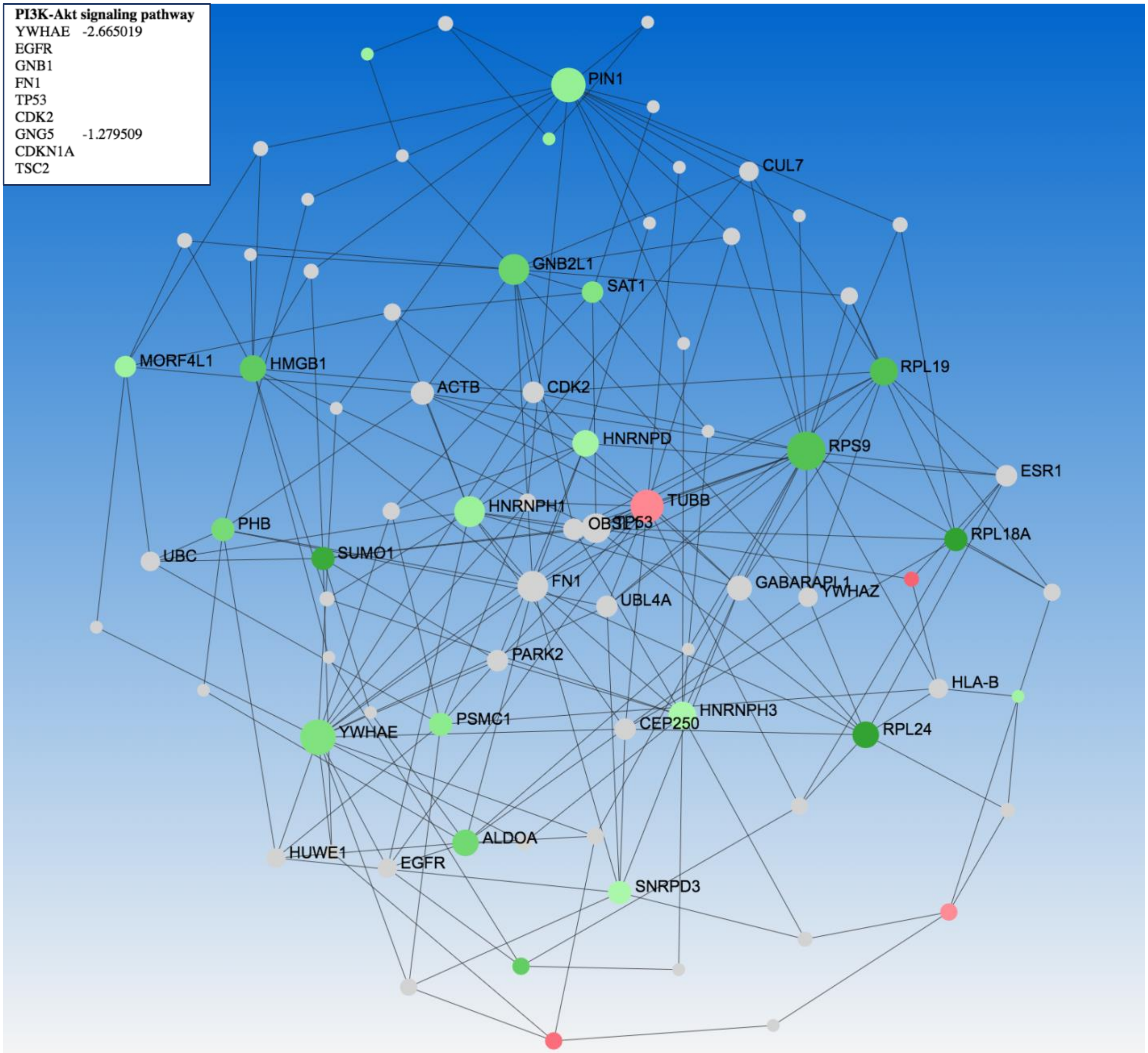

Fig. 17: Minimum Gene Network of the 50 most significantly dysregulated transcripts in the Male Growth-Restricted vs. Female Growth-Restricted comparison of fetal lamb perirenal fat ranked (greatest P-adj =2.67e^{-27}) showing adipose tissue specific PPI. Sheep transcripts were converted to human orthologs and represented as proteins. The size of the circle represents betweenness, the color denotes expression where red is upregulated and green is downregulated, and edges between nodes indicate relationships between proteins. The most significant KEGG pathway is in the top left.

Name	Strand	Start	*p*-value	Sites
14. TRIP12	+	511	5.18e-13	CAAAGATTTC TACTTTTTTTTTTTTTTTTTT GAATTGGGAG
1. GREB1	-	281	1.04e-12	TAATCAATGT GATTTTTTTTTTTTTTTTTTT GGTAGCAGCT
8. AADAC	-	151	5.59e-12	TCTGTGTTCC GGCTTTGTTTTTTTTTTTTTT TTTCCCCTTG
6. ENSOART00020012574	-	459	6.04e-10	AGGCTGGCTT GACTATGTTTTCTTTTTTTTT TAAAGAAACT
11. HSPA6	-	200	9.65e-10	ATTTTAACAT TTCTTTTTTCTGTTTTTTTCT TTAATTCAAC
7. NDUFB3	-	27	1.05e-9	TAATGTGTCT GAGTAGTTTTTTTGTTTTTTT CCCCCTGTTG
17. MACROD1	-	353	1.35e-9	GAATTGGGGT GGTGTTTTTCTTTATATTTTT CCTATATTTT
3. MICOS10	-	796	1.76e-9	CTTTCCGGGG TTTTTGGGTTTTTTTTTTTTT GGCAATTGGT
10. SEC24B	-	916	2.48e-9	AGAGGAACCC GGGGTTTGTCTTTGTTTTTTT AATCTTGAGG
5. ENSOART00020011190	+	874	2.88e-9	AGGAGAGCAT GACTTGTCTCTTTATTTTTCT CTCTTTTTTA
12. SIMC1	+	271	4.29e-8	GTTCCTTCGC TGCTTCTCTTTGTGCATTTTT TCCCAATCTC
9. ENSOART00020021052	+	300	7.67e-8	TATATCAACT TGTTTTTTCCTCCTTATTATT CCCATTTTAT

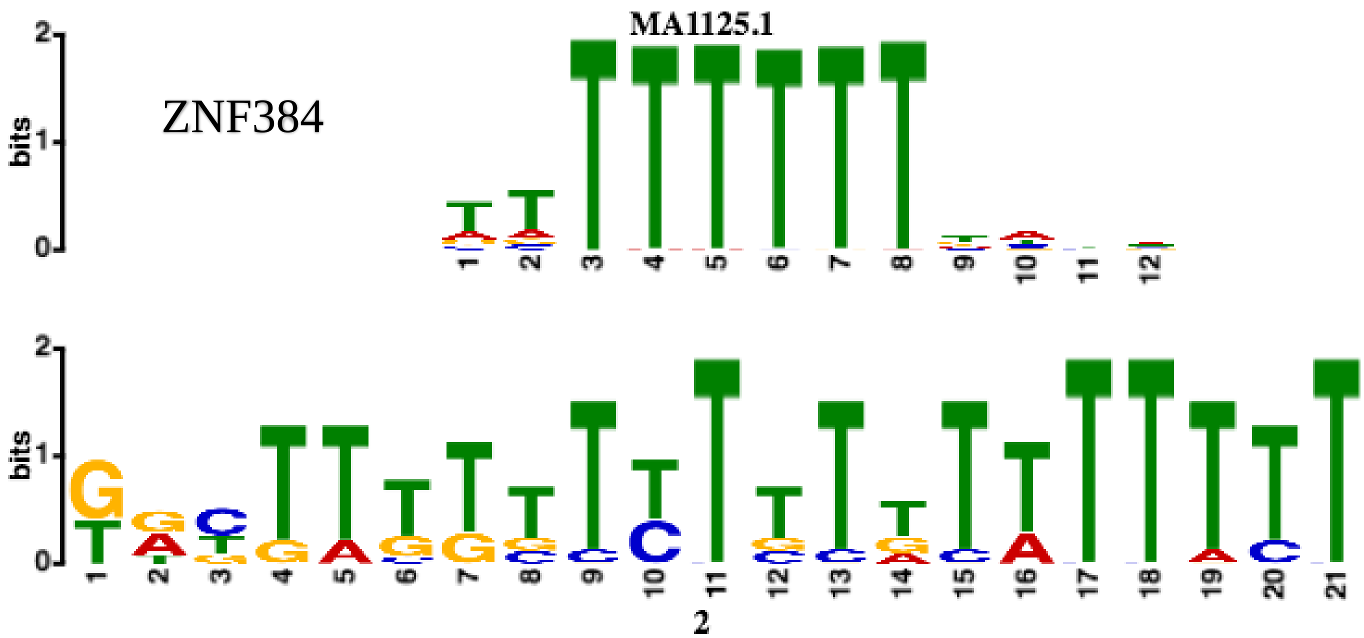

Fig. 18: Demonstrates a common motif in 1000 base pairs upstream of the transcription start site of significantly different transcripts between all four groups. Strand denotes the sense and antisense DNA sequence. The start denotes the number of base pairs upstream to the transcriptional start site. P-value denotes the probability that the presence of motif is by chance in the given sequence as a part of a group of sequences altered by FGR and/or sex. The bottom of the figure shows the common binding motif and the middle of the figure shows a cis-regulatory element of this motif, Zinc-like finger ZNF384. Bits refer to the likelihood that the presence of a particular letter of a specific motif, at a specific site, is in background sequences of transcripts altered by FGR and/or sex.

Name	Strand	Start	*p*-value	Sites
4. ENSOART00020011190	+	586	1.69e-15	CTTGGGGATT TGGGGAGAGGATAGAGGAATGAACGGCCCAGTGTT TTTATTATCT
5. ENSOART00020012574	-	964	9.88e-15	GA TGGCGACTGGAGGGAGGCGACAGCGGCGCTGGCTT AGCAGGAGCC
3. ENSOART00020028276	-	523	5.35e-13	TTTTCTCTTC TGGGGTGAGGAGGCAGTAATGCCCTGCTGGGGGCT GCGCTCACCT
2. NDUFB3	-	316	9.68e-13	GTGGCGCTGG CGGAGACCGGAGAGAGGCGGGAGCAAGACGGTATT GTGAAGGCTG
1. MICOS10	+	576	1.19e-12	AAAGCCAAGG TGAGGCGACGAAGGAAGAGACCGTAGCGCGGTGCC CTCACTCGCC

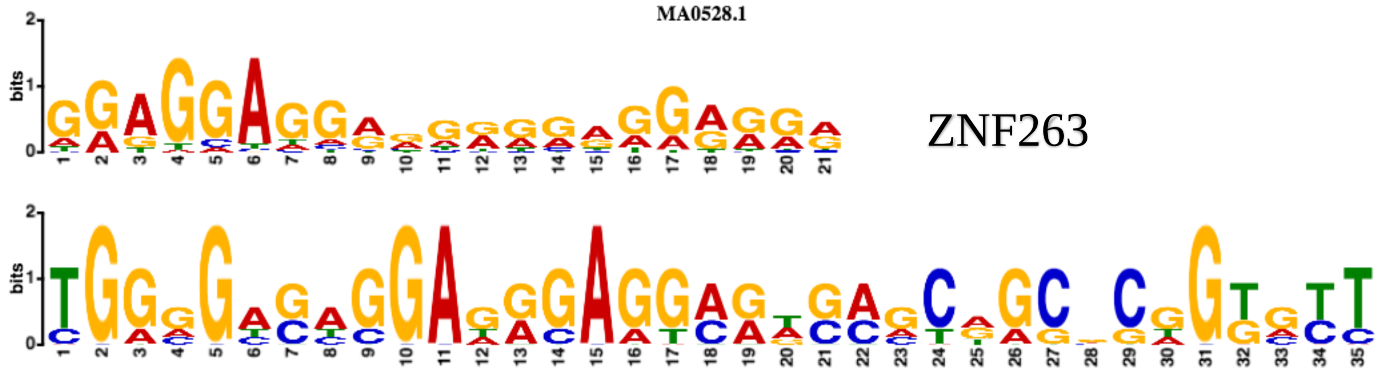

Fig. 19: Demonstrates a common motif in 1000 base pairs upstream of the transcription start site of significantly different transcripts between sexes. Strand denotes the sense and antisense DNA sequence. The start denotes the number of base pairs upstream to the transcriptional start site. P-value denotes the probability that the presence of motif is by chance in the given sequence as a part of a group of sequences altered by sex. The bottom of the figure shows the common binding motif and the middle of the figure shows a cis-regulatory element for this motif, ZNF263. Bits refer to the likelihood that the presence of a particular letter of a specific motif, at a specific site, is in background sequences of genes altered by sex.

Name	Strand	Start	p-value	Sites
4. GREB1	+	2	9.81e-27	C TGCAGTCCATGGGGTCGCGAAGAGTTGGACACGACTGAGTGACT TCACTTTCAC
2. AADAC	+	1	8.35e-26	TGCAGTCCATGGAGTCACAAAGAGACGGACACAACTGAGTGACT GAACAACAAT

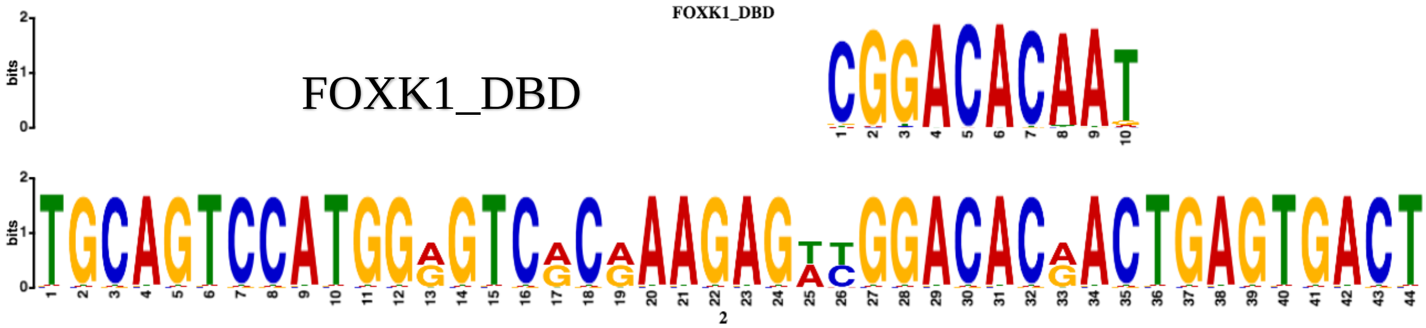

Fig. 20: Demonstrates a common motif in 1000 base pairs upstream of the transcription start site of significantly different transcripts between FGR and control males. Strand denotes the sense and antisense DNA sequence. The start denotes the number of base pairs upstream to the transcriptional start site. P-value denotes the probability that the presence of a motif is by chance in the given sequence as a part of a group of sequences altered by FGR in females. The bottom of the figure shows the common binding motif and the middle of the figure is the cis-regulatory element for this motif, FOX1_DBD. Bits refer to the likelihood that the presence of a particular letter of a specific motif, at a specific site, is in background sequences of transcripts altered by FGR in males.

8. AADAC	-	224	2.00e-28	TGGATAGATG AGCCTGGCAGGCTACAGTCCATGGGGTTGCAAAGAGTCGGACATGACTGA GCAAGCAAAA
17. MACROD1	+	62	2.78e-27	AGGACAGGGA AGCCTGGTGTGCTGCAGTCCATGGGGTGGCAAAGAGTTGGACACGACTGA GCAACTGAAC
1. GREB1	+	124	2.28e-25	GGGATGGGGG AGCCTGGTAGGCTGCCGTCCATGGGGTCACACAGAGTCGGACACGACTGA AGCGACTTAG
5. ENSOART00020011190	+	101	4.53e-24	TGGACAGGGA AGTCTGGCATGCTGCAATTCATGGGGTTGCAAAAAGTTGGACATGACTGA ACGACTGAAC
14. TRIP12	+	776	3.95e-22	ATGGGCAGAG GAGCCTGTGGTCTATAGTCCATGGGGTCACAAAGAATTGAACATGACTGA GCAACACTTT
11. HSPA6	-	494	2.30e-17	TGGTTGGTTG AAGAGGGCGGTTTTGAGTCCAGCGGCTCGAGAAAAACCGAAAGCAATAGA GCCGTGGCTT

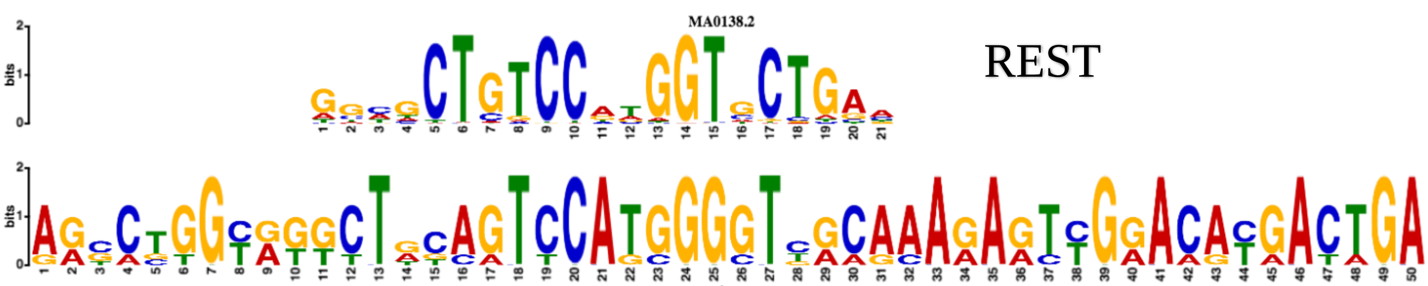

Fig. 21: Demonstrates a common motif in 1000 base pairs upstream of the transcription start site of significantly different transcripts between FGR and control females. Strand denotes the sense and antisense DNA sequence. The start denotes the number of base pairs upstream to the transcriptional start site. P-value denotes the probability that the presence of a motif is by chance in the given sequence as a part of a group of sequences altered by FGR in females. The bottom of the figure shows the common binding motif and the middle of the figure shows the cis-regulatory element for this motif, REST. Bits refer to the likelihood that the presence of a particular letter of a specific motif, at a specific site, is in background sequences of genes altered by FGR in females.

Table 1

Symbol	Human Gene ID	Sheep Transcript ID	♂ Vs ♀ Ctrl FC	P-adj	Vs. ⚥ Ctrl FC	P-adj.
NDUFB3	ENSG00000119013	ENSOART00020026250	-20.75	$3.15E^{-182}$	-25.04	$9.01E^{-200}$
***GOLM2**	Novel	ENSOART00020028276	-10.26	$5.78E^{-153}$	-8.52	$5.98E^{-126}$
MICOS10	ENSG00000173436	ENSOART00020011224	-12.67	$2.58E^{-145}$	-8.52	$3.30E^{-102}$
***SARNP**	Novel	ENSOART00020011190	-65.70	$1.11E^{-133}$	-34.36	2.01E-^{115}
DACT1	Novel	ENSOART00020012574	-221.60	$2.73E^{-132}$	186.35	$9.24E^{-120}$

Table 1: Top 5 significantly different transcripts between sexes in Control and Growth-Restricted fetal lamb perirenal fat (P-adj <0.05, log2FC>|1.5|). All 5 were shared between Growth-Restricted and Control fetal lamb perirenal fat. FC=FoldChange.

Table 2

Symbol	Human Gene ID	Sheep Transcript ID	♂ FGR vs Ctrl FC	P-adj.	♀ FGR vs Ctrl FC	P-adj.
GREB1	ENSG00000196208	ENSOART00020018468	-7.63	$1.84E^{-11}$	-	-
PCK2	ENSG00000100889	ENSOART00020016887	3.22	$1.61E^{-10}$	-	-
AADAC	ENSG00000114771	ENSOART00020005588	-6.70	$2.08E^{-9}$	-	-
***RPL12**	Novel	ENSOART00020021052	169.25	$5.64E^{-8}$	-	-
***PTK6**	Novel	ENSOART00020005697	1.75	$2.95E^{-8}$	1.51	0.0008
SEC24B	ENSG00000138802	ENSOART00020037913	-	-	2.53	0.0001
MACROD1	ENSG00020024720	ENSOART00020038713	-	-	1.3	0.001
SIMC1	ENSG00000170085	ENSOART00020030830	-	-	3.63	0.0021
PMPCA	ENSG00020002792	ENSOART00020004296	-	-	1.51	0.0038

Table 2: Top 5 Significantly different transcripts between Growth-Restricted and Control fetal lamb perirenal fat from both sexes (P-adj <0.05, log2FC>|1.5|). Two transcripts did not make the cut-off for log2FC for the Female Growth-Restricted vs. Control fetal perirenal fat comparison and are denoted by *. FC=FoldChange.

Table 3

Group Comparison	Upregulated	Downregulated	Total
MFGR_MC	343	203	546
FFGR_FC	9	4	13
MC_FC	1635	1466	3101
MFGR_FFGR	1583	1587	3170

Table 3: Significantly different transcripts determined by RNAseq analysis using DESEQ2 package in R-studio (P-adj < 0.05). MC – Male Control, FC – Female Control, MFGR – Male Fetal Growth-Restricted, FFGR – Female Fetal Growth-Restricted.

Table 4

GSE Accession	Project number	RNAseq Folder	Description of Study	Significance	Title
GSE137022	SRP220671	Study 1 (RNAseq3)	RNA isolated from visceral adipose tissue demonstrating significant differential gene expression between mice given a HFD and CHOW in males and females (P-adj<0).	This study demonstrates significant sexual dimorphism in healthy and obese mouse VAT.	RNA-seq from adipose and liver tissue in Fam13a knockout and wildtype mice on different diets
GSE121836	SRP166940	Study 2 (RNAseq8)	RNA isolated from three different visceral adipose depots demonstrating significant differential gene expression between male and female mice (P-adj<0).	This study demonstrates significant sex differences in three different depots of VAT in mice.	Sex-specific adipose tissue imprinting of regulatory T cells (RNA-seq)
GSE151358	SRP265091	Study 3 (RNAseq11)	RNA from mouse inguinal adipose tissue from male and female controls and MHSD and FHSD (P-adj<0).	This study demonstrates significant differences between sexes but not between HSD and controls.	RNA-seq from adipose and liver tissue in Fam13a knockout and wildtype mice on different diets
GSE168387	SRP309581	Study 4 (RNAseq9)	RNA from human induced pluripotent brown adipocytes at different stages of differentiation from males and females (P-adj<0).	This study demonstrates significant sex differences human brown adipocytes.	Unravelling the developmental roadmap towards human brown adipose tissue
GSE166047	SRP304398	Study 5 (RNAseq10)	RNA from human SAT from normal weight females and from obese and T2D males and females (P-adj<0).	This study demonstrates significant differences between NWF and OBM, and between T2DOBF and OBM. There was not significant difference between OBM and OBF.	Transcriptional deregulation in subcutaneous adipose tissue from severely obese patients is associated with cancer: focus on gender differences and role of type 2 diabetes
GSE112947	SRP139376	Study 6 (RNAseq7)	RNA isolated from visceral adipose tissue demonstrating significant differential gene expression between MHFSD mice and CHOW males (P-value<0.5).	This study demonstrates significant differences between MHFD mice compared to MCHOW but not between sexes or between FHFD and FCHOW.	Gene-by-sex interactions in mitochondrial functions and tissue-specific gene expression in cardio-metabolic traits
GSE137869	SRP222987	Study 7 (RNA seq6)	RNA isolated from visceral adipose tissue demonstrating significant differential gene expression between calorie restricted, CHOW, and HFD in young and old rats (P-adj<0.5).	This study suggests significant differences in healthy, obese, and underweight rat VAT.	Caloric restriction reprograms the single-cell transcriptional landscape of Rattus norvegicus aging
GSE124772	SRP176481	Study 8 (RNAseq4)	RNA isolated from visceral adipose tissue demonstrating differential gene expression between mice 21 months apart in age (P-adj<0.5)	This study demonstrates significant differences in young mouse VAT compared to aging mouse VAT.	A nutritional memory impairs transcriptional, metabolic and survival response to dietary restriction in old mice

Table 4: Description of GSEs used in Comparative Analysis to determine conserved transcripts across sheep, human, mouse, and rat including link to GSE and SRP htmls. Each study was chosen based on its relevance to the current study. Key Words in Ensembl search engine: *Visceral Adipose Tissue, Intrauterine-Growth Restriction, Illumina (platform), and obesity*.

Table 5

GSE	Groups	Upregulated	Downregulated	Total
GSE137022	MHFD_FHFD	6920	3359	10279
GSE121836	Epid_Perio	5648	2721	8369
GSE121836	MSVF_FSVF	12582	15457	28039
GSE121836	M.ing_F.ing	5832	6092	11924
GSE151358	M.AL_F.AL	1421	2190	3611
GSE168387	M_F	26949	22109	49058
GSE166047	OBM_T2DOBF	425	589	1014
GSE166047	OBM_NWF	3094	2981	6075

Table 5: Significantly different transcripts in comparative analyses investigating differences in fetal neonatal visceral fat between sexes determined by RNAseq analysis using DESEQ2 package in R-studio (P-adj < 0.05). MC – Male Control, FC – Female Control, MFGR – Male Fetal Growth-Restricted, FFGR – Female Fetal Growth-Restricted.

Table 6

GSE	Groups	Upregulated	Downregulated	Total
GSE112947	MHFD_MCHOW	9707	11291	20998
GSE137869	Y.AL_O.AL	2861	3453	6314
GSE137869	O.AL_O.CR	1700	2022	3722
GSE137869	Y.AL_O.CR	1649	2073	3722
GSE124772	5mo_26mo	478	636	1114
GSE166047	OBM_T2DOBF	425	589	1014
GSE166047	OBM_NWF	3094	2981	6075

Table 6: Significantly different transcripts in comparative analyses investigating differences in fetal neonatal visceral fat between obese/FGR models and control fetal or neonatal visceral fat determined by RNAseq analysis using DESEQ2 (P-adj < 0.05). MC – Male Control, FC – Female Control, MFGR – Male Fetal Growth Restricted, FFGR – Female Fetal Growth Restricted.

Table 7

GSE	Animal Model	Group	MFGR	FFGR	MC	FC	Total
GSE137022	HFD Mouse	MHFD	23	17	25	14	79
GSE137022	HFD Mouse	FHFD	7	6	7	7	27
GSE137022	WT mouse	MCHOW	30	1	15	0	46
GSE137022	HFD mouse	MHFD	35	0	47	2	84
GSE121836	Mouse	M.epid	22	21	28	15	86
GSE121836	Mouse	F.perio	1	9	3	7	20
GSE121836	Mouse	M.SVF	326	170	245	190	931
GSE121836	Mouse	F.SVF	175	283	329	190	977
GSE121836	Mouse	M.ingui	171	121	110	147	549
GSE121836	Mouse	F.ingui	70	96	85	49	300
GSE151358	Mouse	M_AL	15	33	11	37	96
GSE151358	Mouse	F_AL	16	23	31	17	87
GSE168387	Human Brown Adipocytes	Male	319	359	290	345	1313
GSE168387	Human Brown Adipocytes	Female	281	231	292	182	986
GSE166047	Human SAT	OBM	1	3	1	0	5
GSE166047	Human SAT	T2DOBF	1	7	2	5	15
GSE166047	Human SAT	OBM	31	13	30	13	87
GSE166047	Human SAT	NWF	23	44	13	47	127
		Total	1547	1437	1564	1267	

Table 7: Common significantly upregulated transcripts in fetal or neonatal visceral fat shared between males and females in comparative analyses and males and females in the current study determined by RNAseq analysis using DESEQ2 (P-adj < 0.05). MC – Male Control, FC – Female Control, MFGR – Male Fetal Growth Restricted, FFGR – Female Fetal Growth Restricted. Blue represents shared transcripts between males and grey represents shared transcripts between females that follow the trend of sexual dimorphism in adipose tissue programming.

Table 8

GSE	Animal Model	Group	MFGR	FFGR	MC	FC	Total
GSE137022	HFD Mouse	MHFD	6	7	7	7	27
GSE137022	HFD Mouse	FHFD	17	23	14	25	79
GSE137022	WT mouse	MCHOW	47	2	35	0	84
GSE137022	HFD mouse	MHFD	15	0	30	1	46
GSE121836	Mouse	M.epid	9	1	7	3	20
GSE121836	Mouse	F.perio	21	22	15	28	86
GSE121836	Mouse	M.SVF	283	175	190	329	977
GSE121836	Mouse	F.SVF	170	326	190	245	931
GSE121836	Mouse	M.ingui	96	70	49	85	300
GSE121836	Mouse	F.ingui	121	171	147	110	549
GSE151358	Mouse	M_AL	23	16	17	31	87
GSE151358	Mouse	F_AL	33	15	37	11	96
GSE168387	Human Brown Adipocytes	Male	231	281	182	292	986
GSE168387	Human Brown Adipocytes	Female	359	319	345	290	1313
GSE166047	Human SAT	OBM	7	1	5	2	15
GSE166047	Human SAT	T2DOBF	3	1	0	1	5
GSE166047	Human SAT	OBM	44	23	47	13	127
GSE166047	Human SAT	NWF	13	31	13	30	87
		Total	841	828	738	875	

Table 8: Common significantly downregulated transcripts in fetal or neonatal visceral fat shared between males and females in comparative analyses and males and females in the current study determined by RNAseq analysis using DESEQ2 (P-adj < 0.05). MC – Male Control, FC – Female Control, MFGR – Male Fetal Growth Restricted, FFGR – Female Fetal Growth Restricted. Blue represents shared transcripts between males and grey represents shared transcripts between females that follow a trend of sexual dimorphism in adipose tissue programming.

Table 9

GSE	Animal Model	Group	MFGR	FFGR	MC	FC	Total
GSE112947	WT mouse	MCHOW	34	9	21	0	64
GSE112947	HFD mouse	MHFSD	63	0	41	18	122
GSE137869	Ad libitum rat	Y_AL	14	0	19	0	33
GSE137869	Calorie restricted rat	O_CR	36	0	6	0	42
GSE137869	Young rat	Y_AL	37	0	30	1	68
GSE137869	Aging rat	O_AL	58	0	15	0	73
GSE137869	WT rat	O_AL	19	0	71	1	91
GSE137869	Calorie restricted rat	O_CR	31	0	75	0	106
GSE124772	Young mouse	month5	4	0	2	2	8
GSE124772	Aging mouse	month26	2	0	2	0	4
GSE166047	Human SAT	OBM	1	3	1	0	5
GSE166047	Human SAT	T2DOBF	1	7	2	5	15
GSE166047	Human SAT	OBM	31	13	30	13	87
GSE166047	Human SAT	NWF	23	44	13	47	127
		Total	34	9	21	0	845

Table 9: Common significantly upregulated transcripts in fetal or neonatal visceral fat shared between FGR and/or obese models in comparative analyses and MFGR and FFGR in the current study determined by RNAseq analysis using DESEQ2 (P-adj < 0.05). MC – Male Control, FC – Female Control, MFGR – Male Fetal Growth Restricted, FFGR – Female Fetal Growth Restricted. Blue represents shared transcripts between obese models and FGR and grey represents shared transcripts between controls and WT that follow the trend of FGR-mediated adipose tissue programming.

Table 10

GSE	Animal Model	Group	MFGR	FFGR	MC	FC	Total
GSE112947	WT mouse	MCHOW	41	18	63	0	122
GSE112947	HFD mouse	MHFSD	21	0	34	9	64
GSE137869	Ad libitum rat	Y_AL	6	0	36	0	42
GSE137869	Calorie restricted rat	O_CR	19	0	14	0	33
GSE137869	Young rat	Y_AL	15	0	58	0	73
GSE137869	Aging rat	O_AL	30	1	37	0	68
GSE137869	WT rat	O_AL	75	0	31	0	106
GSE137869	Calorie restricted rat	O_CR	71	1	19	0	91
GSE124772	Young mouse	month5	2	0	2	0	4
GSE124772	Aging mouse	month26	2	0	4	2	8
GSE166047	Human SAT	OBM	7	1	5	2	15
GSE166047	Human SAT	T2DOBF	3	1	0	1	5
GSE166047	Human SAT	OBM	44	23	47	13	127
GSE166047	Human SAT	NWF	13	31	13	30	87
		Total	**1987**	**1552**	**4330**	**2250**	**845**

Table 10: Common significantly downregulated transcripts in fetal or neonatal visceral fat shared between FGR and/or obese models in comparative analyses and MFGR and FFGR in the current study determined by RNAseq analysis using DESEQ2 (P-adj < 0.05). MC – Male Control, FC – Female Control, MFGR – Male Fetal Growth Restricted, FFGR – Female Fetal Growth Restricted. Blue represents shared transcripts between obese models and FGR and grey represents shared transcripts between controls and WT that follow the trend of FGR-mediated adipose tissue programming.

Table 11

Pathway	Total	Expected	Hits	P.Value	FDR
FoxO signaling pathway	132	0.751	6	9.12E-05	0.029*
Colorectal cancer	86	0.489	4	0.00138	0.101
Breast cancer	147	0.836	5	0.00138	0.101
TGF-beta signaling pathway	92	0.523	4	0.00177	0.101
Jak-STAT signaling pathway	162	0.921	5	0.00212	0.101
Prostate cancer	97	0.552	4	0.00215	0.101
Notch signaling pathway	48	0.273	3	0.00248	0.101
Pathways in cancer	530	3.01	9	0.00253	0.101
Endometrial cancer	58	0.33	3	0.00426	0.15
Cell cycle	124	0.705	4	0.0052	0.161
Mitophagy - animal	65	0.37	3	0.00586	0.161
MAPK signaling pathway	295	1.68	6	0.00608	0.161
Ubiquitin mediated proteolysis	137	0.779	4	0.00738	0.165
Estrogen signaling pathway	138	0.785	4	0.00757	0.165
Adherens junction	72	0.409	3	0.00779	0.165
Chronic myeloid leukemia	76	0.432	3	0.00904	0.18
Hepatitis C	155	0.881	4	0.0113	0.205
Wnt signaling pathway	158	0.899	4	0.0121	0.205
ErbB signaling pathway	85	0.483	3	0.0123	0.205
Hepatitis B	163	0.927	4	0.0134	0.206
Protein processing in endoplasmic reticulum	165	0.938	4	0.014	0.206
PI3K-Akt signaling pathway	354	2.01	6	0.0143	0.206
Endocrine resistance	98	0.557	3	0.0179	0.248
Bladder cancer	41	0.233	2	0.0225	0.298
Viral carcinogenesis	201	1.14	4	0.0267	0.327
Proteoglycans in cancer	201	1.14	4	0.0267	0.327
Thyroid hormone signaling pathway	116	0.66	3	0.0279	0.328
Hedgehog signaling pathway	47	0.267	2	0.0291	0.33
Malaria	49	0.279	2	0.0314	0.344
Signaling pathways regulating pluripotency of stem cells	139	0.79	3	0.044	0.452
Fluid shear stress and atherosclerosis	139	0.79	3	0.044	0.452

Table 11: Top KEGG Enriched Pathways on Network Analyst for the Male Growth-Restricted vs. Control comparison. The one significant pathway was the FoxO signaling pathway (P-adj <0.05)**.** The top 50 sheep transcripts were converted to human transcripts on Ensembl Biomart to account for additional gene coverage in human genome database. P-value and FDR were calculated by Network Analyst.

Table 12

Pathway	Total	Expected	Hits	P.Value	FDR
Estrogen signaling pathway	138	0.196	3	0.000825	0.262
Prolactin signaling pathway	70	0.0995	2	0.00421	0.669
Endocrine resistance	98	0.139	2	0.00811	0.859
Breast cancer	147	0.209	2	0.0176	1
Protein processing in endoplasmic reticulum	165	0.235	2	0.0219	1
Focal adhesion	199	0.283	2	0.0311	1
Ras signaling pathway	232	0.33	2	0.0412	1
Autophagy - other	32	0.0455	1	0.0446	1
Regulation of lipolysis in adipocytes	55	0.0782	1	0.0755	1
Legionellosis	55	0.0782	1	0.0755	1

Table 12: Top KEGG Enriched Pathways on Network Analyst for the Female Growth-Restricted vs. Female Control Comparison (P-adj<0.05*). The top 50 sheep transcripts were converted to human transcripts on Ensembl Biomart to account for additional gene coverage in human genome database. P-value and FDR were calculated by Network Analyst. No pathways were significant.

Table 13

Pathway	Total	Expected	Hits	P.Value	FDR
Bladder cancer *	41	0.233	6	9.21E-08	2.55E-05
Hepatitis C *	155	0.881	9	1.60E-07	2.55E-05
PI3K-Akt signaling pathway *	354	2.01	12	3.91E-07	4.15E-05
Kaposi's sarcoma-associated herpesvirus infection *	186	1.06	9	7.58E-07	4.91E-05
Endometrial cancer *	58	0.33	6	7.71E-07	4.91E-05
Colorectal cancer *	86	0.489	6	7.96E-06	0.000422
Small cell lung cancer *	93	0.529	6	1.25E-05	0.000569
HIF-1 signaling pathway *	100	0.569	6	1.90E-05	0.000756
Pathways in cancer *	530	3.01	12	2.62E-05	0.000796
Cellular senescence *	160	0.91	7	2.86E-05	0.000796
Central carbon metabolism in cancer *	65	0.37	5	3.02E-05	0.000796
Hepatitis B *	163	0.927	7	3.22E-05	0.000796
Non-small cell lung cancer *	66	0.375	5	3.25E-05	0.000796
Melanoma *	72	0.409	5	4.97E-05	0.00111
Thyroid cancer *	37	0.21	4	5.24E-05	0.00111
Pancreatic cancer *	75	0.427	5	6.05E-05	0.00113
Glioma *	75	0.427	5	6.05E-05	0.00113
Chronic myeloid leukemia *	76	0.432	5	6.45E-05	0.00114
ErbB signaling pathway *	85	0.483	5	0.00011	0.00169
Ubiquitin mediated proteolysis *	137	0.779	6	0.000112	0.00169
Epstein-Barr virus infection *	201	1.14	7	0.000122	0.00169
Viral carcinogenesis *	201	1.14	7	0.000122	0.00169

Proteoglycans in cancer *	201	1.14	7	0.000122	0.00169
Breast cancer *	147	0.836	6	0.000165	0.00219
Prostate cancer *	97	0.552	5	0.000206	0.00256
Endocrine resistance *	98	0.557	5	0.000216	0.00256
MAPK signaling pathway *	295	1.68	8	0.000217	0.00256
Thyroid hormone signaling pathway *	116	0.66	5	0.000473	0.00537
Neurotrophin signaling pathway *	119	0.677	5	0.000532	0.00583
Renal cell carcinoma *	69	0.392	4	0.000601	0.00637
Cell cycle *	124	0.705	5	0.000642	0.00659
Autophagy – animal *	128	0.728	5	0.000742	0.00737
Apelin signaling pathway *	137	0.779	5	0.00101	0.00972
MicroRNAs in cancer *	299	1.7	7	0.00134	0.0125
HTLV-I infection *	219	1.25	6	0.00138	0.0125
Gap junction *	88	0.5	4	0.0015	0.0132
Ribosome *	153	0.87	5	0.00165	0.0142
Choline metabolism in cancer *	99	0.563	4	0.00231	0.0194
Alcoholism *	180	1.02	5	0.00336	0.0274
Serotonergic synapse *	115	0.654	4	0.00398	0.0316
VEGF signaling pathway *	59	0.336	3	0.00447	0.0347
Acute myeloid leukemia *	66	0.375	3	0.00612	0.0463
Natural killer cell mediated cytotoxicity *	131	0.745	4	0.00631	0.0467
FoxO signaling pathway *	132	0.751	4	0.00648	0.0469

Table 13: Top KEGG Downregulated Enriched Pathways on Network Analyst for Male vs. Female Control Comparison (P-adj<0.05). The top 50 sheep transcripts were converted to human transcripts on Ensembl Biomart to account for additional gene coverage in human genome database.

Table 14

Pathway	Total	Expected	Hits	P.Value	FDR
PI3K-Akt signaling pathway *	354	2.33	14	3.77E-08	6.53E-06
Hepatitis C *	155	1.02	10	4.92E-08	6.53E-06
Colorectal cancer *	86	0.567	8	7.23E-08	6.53E-06
Endometrial cancer *	58	0.382	7	8.22E-08	6.53E-06
Bladder cancer *	41	0.27	6	2.29E-07	1.45E-05
Proteoglycans in cancer *	201	1.32	10	5.65E-07	3.00E-05
Cellular senescence *	160	1.05	9	7.99E-07	3.63E-05
Hepatitis B *	163	1.07	9	9.34E-07	3.71E-05
FoxO signaling pathway *	132	0.87	8	1.99E-06	7.05E-05
Kaposi's sarcoma-associated herpesvirus infection *	186	1.23	9	2.81E-06	8.20E-05
Prostate cancer *	97	0.639	7	2.89E-06	8.20E-05
Endocrine resistance *	98	0.646	7	3.09E-06	8.20E-05
Non-small cell lung cancer *	66	0.435	6	4.08E-06	9.97E-05
Breast cancer *	147	0.969	8	4.48E-06	0.000102

Pathways in cancer *	530	3.49	14	5.14E-06	0.000109
Pancreatic cancer *	75	0.494	6	8.64E-06	0.000162
Glioma *	75	0.494	6	8.64E-06	0.000162
Chronic myeloid leukemia *	76	0.501	6	9.33E-06	0.000165
Cell cycle *	124	0.817	7	1.48E-05	0.000247
ErbB signaling pathway *	85	0.56	6	1.78E-05	0.000284
Viral carcinogenesis *	201	1.32	8	4.40E-05	0.000667
Central carbon metabolism in cancer *	65	0.428	5	6.24E-05	0.000902
Renal cell carcinoma *	69	0.455	5	8.33E-05	0.00115
Thyroid cancer *	37	0.244	4	9.42E-05	0.00125
Melanoma *	72	0.475	5	0.000102	0.00127
Thyroid hormone signaling pathway *	116	0.765	6	0.000104	0.00127
Endocytosis *	244	1.61	8	0.000172	0.00202
Apelin signaling pathway *	137	0.903	6	0.000258	0.00294
Fc gamma R-mediated phagocytosis *	91	0.6	5	0.000309	0.00339
Small cell lung cancer *	93	0.613	5	0.000342	0.00362
Phospholipase D signaling pathway *	148	0.976	6	0.000392	0.00402
Choline metabolism in cancer *	99	0.653	5	0.000457	0.00454
HTLV-I infection *	219	1.44	7	0.000531	0.00511
Jak-STAT signaling pathway *	162	1.07	6	0.000634	0.00593
MicroRNAs in cancer *	299	1.97	8	0.000677	0.00615
Ras signaling pathway *	232	1.53	7	0.000748	0.00661
Acute myeloid leukemia *	66	0.435	4	0.000893	0.00768
Neurotrophin signaling pathway *	119	0.784	5	0.00106	0.00884
Prolactin signaling pathway *	70	0.461	4	0.00111	0.00909
p53 signaling pathway *	72	0.475	4	0.00124	0.00985
Platinum drug resistance *	73	0.481	4	0.0013	0.0101
Chemokine signaling pathway *	190	1.25	6	0.00146	0.0108
Autophagy – animal *	128	0.844	5	0.00146	0.0108
EGFR tyrosine kinase inhibitor resistance *	79	0.521	4	0.00175	0.0126
Epstein-Barr virus infection *	201	1.32	6	0.00194	0.0137
Estrogen signaling pathway *	138	0.91	5	0.00204	0.0141
Signaling pathways regulating pluripotency of stem cells *	139	0.916	5	0.00211	0.0143
Gap junction *	88	0.58	4	0.0026	0.0172
Regulation of actin cytoskeleton *	214	1.41	6	0.00266	0.0173
MAPK signaling pathway *	295	1.94	7	0.00299	0.019
GnRH signaling pathway *	93	0.613	4	0.00318	0.0192
Ribosome *	153	1.01	5	0.0032	0.0192
Oxytocin signaling pathway *	153	1.01	5	0.0032	0.0192
HIF-1 signaling pathway *	100	0.659	4	0.00412	0.0243

Pathogenic Escherichia coli infection *	55	0.363	3	0.00556	0.0322
Alcoholism *	180	1.19	5	0.00637	0.0362
Serotonergic synapse *	115	0.758	4	0.00676	0.0377
Mitophagy – animal *	65	0.428	3	0.00884	0.0477
Shigellosis *	65	0.428	3	0.00884	0.0477
Oocyte meiosis *	125	0.824	4	0.00904	0.0479

Table 14: Top KEGG Enriched Pathways on Network Analyst for Male vs. Female Growth-Restricted Comparison (P-adj<0.05). The top 50 sheep transcripts were converted to human transcripts on Ensembl Biomart to account for additional gene coverage in human genome database.

References

1. Organization, W.H., *Obesity*. 2020.
2. Tremmel, M., et al., *Economic Burden of Obesity: A Systematic Literature Review.* Int J Environ Res Public Health, 2017. **14**(4).
3. Fruh, S.M., *Obesity: Risk factors, complications, and strategies for sustainable long-term weight management.* J Am Assoc Nurse Pract, 2017. **29**(S1): p. S3-S14.
4. Djalalinia, S., et al., *Health impacts of Obesity.* Pak J Med Sci, 2015. **31**(1): p. 239-42.
5. Barker, D.J., *Outcome of low birthweight.* 1994. **42**(4-5): p. 223-230.
6. Hales, C.N. and D.J. Barker, *The thrifty phenotype hypothesis.* Br Med Bull, 2001. **60**: p. 5-20.
7. Goyal, D., S.W. Limesand, and R. Goyal, *Epigenetic responses and the developmental origins of health and disease.* J Endocrinol, 2019. **242**(1): p. T105-T119.
8. Jang, E.A., L.D. Longo, and R. Goyal, *Antenatal maternal hypoxia: criterion for fetal growth restriction in rodents.* Frontiers in Physiology, 2015. **6**(176).
9. Simko, M., et al., *Maternal Body Mass Index and Gestational Weight Gain and Their Association with Pregnancy Complications and Perinatal Conditions.* Int J Environ Res Public Health, 2019. **16**(10).
10. Goyal, R. and L. Longo, *Maternal protein deprivation: sexually dimorphic programming of hypertension in the mouse.* Hypertens Res, 2013. **36**(1): p. 29-35.
11. Dearden, L., S.G. Bouret, and S.E. Ozanne, *Sex and gender differences in developmental programming of metabolism*. Mol Metab, 2018. **15**: p. 8-19.
12. Tchoukalova, Y.D., et al., *Fetal baboon sex-specific outcomes in adipocyte differentiation at 0.9 gestation in response to moderate maternal nutrient reduction.* Int J Obes (Lond), 2014. **38**(2): p. 224-30.
13. Longo, L.D. and R. Goyal, *Cerebral artery signal transduction mechanisms: developmental changes in dynamics and Ca2+ sensitivity.* Curr Vasc Pharmacol, 2013. **11**(5): p. 655-711.
14. Goyal, R., et al., *Cerebral Artery Alpha-1 AR Subtypes: High Altitude Long-Term Acclimatization Responses.* PLoS One, 2014. **9**(11): p. e112784.
15. Goyal, R. and L. Longo, *Acclimatization to long-term hypoxia: gene expression in ovine carotid arteries.* Physiol Genomics, 2014. **46**(19): p. 725-34.
16. Goyal, R., et al., *Antenatal maternal low protein diet: ACE-2 in the mouse lung and sexually dimorphic programming of hypertension.* BMC Physiol, 2015. **15**(1): p. 2.
17. Goyal, R., et al., *Maternal protein deprivation: changes in systemic renin-angiotensin system of the mouse fetus.* Reprod Sci, 2009. **16**(9): p. 894-904.
18. Yates, D.T., et al., *Postnatal beta2 Adrenergic Treatment Improves Insulin Sensitivity in Lambs with IUGR but not Persistent Defects in Pancreatic Islets or Skeletal Muscle.* J Physiol, 2019.
19. Goyal, R., et al., *Antenatal maternal protein deprivation: sexually dimorphic programming of the pancreatic renin-angiotensin system.* J Renin Angiotensin Aldosterone Syst, 2013. **14**(2): p. 137-45.
20. Goyal, R., et al., *Antenatal Maternal Long-Term Hypoxia: Acclimatization Responses with Altered Gene Expression in Ovine Fetal Carotid Arteries.* PLoS ONE, 2013. **8**(12): p. e82200.
21. Goyal, D. and R. Goyal, *Developmental Maturation and Alpha-1 Adrenergic Receptors-Mediated Gene Expression Changes in Ovine Middle Cerebral Arteries.* Sci Rep, 2018. **8**(1): p. 1772.
22. Beatman, E., et al., *West Nile virus growth is independent of autophagy activation.* Virology, 2012. **433**(1): p. 262-272.
23. Zhu, Q., et al., *Apolipoprotein A-IV Enhances Fatty Acid Uptake by Adipose Tissues of Male Mice via Sympathetic Activation.* Endocrinology, 2020. **161**(4).

24. Saely, C.H., K. Geiger, and H. Drexel, *Brown versus white adipose tissue: a mini-review.* Gerontology, 2012. **58**(1): p. 15-23.
25. Giralt, M. and F. Villarroya, *White, brown, beige/brite: different adipose cells for different functions?* Endocrinology, 2013. **154**(9): p. 2992-3000.
26. Villarroya, F., et al., *Inflammation of brown/beige adipose tissues in obesity and metabolic disease.* J Intern Med, 2018. **284**(5): p. 492-504.
27. Sarjeant, K. and J.M. Stephens, *Adipogenesis.* Cold Spring Harb Perspect Biol, 2012. **4**(9): p. a008417.
28. Gimble, J.M., A.J. Katz, and B.A. Bunnell, *Adipose-Derived Stem Cells for Regenerative Medicine.* Circulation Research, 2007. **100**(9): p. 1249-1260.
29. Mohamad Buang, M.L., et al., *In vitro generation of functional insulin-producing cells from lipoaspirated human adipose tissue-derived stem cells.* Arch Med Res, 2012. **43**(1): p. 83-8.
30. Joo, H.J., J.H. Kim, and S.J. Hong, *Adipose Tissue-Derived Stem Cells for Myocardial Regeneration.* Korean Circ J, 2017. **47**(2): p. 151-159.
31. Huang, T., et al., *Neuron-like differentiation of adipose-derived stem cells from infant piglets in vitro.* J Spinal Cord Med, 2007. **30 Suppl 1**: p. S35-40.
32. Limesand, S.W., et al., *Diminished β-cell replication contributes to reduced β-cell mass in fetal sheep with intrauterine growth restriction.* American Journal of Physiology-Regulatory, Integrative and Comparative Physiology, 2005. **288**(5): p. R1297-R1305.
33. Limesand, S.W., T.R.H. Regnault, and W.W. Hay, *Characterization of Glucose Transporter 8 (GLUT8) in the Ovine Placenta of Normal and Growth Restricted Fetuses.* Placenta, 2004. **25**(1): p. 70-77.
34. Saito, M., *Brown Adipose Tissue as a Regulator of Energy Expenditure and Body Fat in Humans.* Diabetes Metab J, 2013. **37**(1): p. 22-29.
35. Galan, H.L., et al., *Relationship of fetal growth to duration of heat stress in an ovine model of placental insufficiency.* Am J Obstet Gynecol, 1999. **180**(5): p. 1278-82.
36. Hutch, J.A., R.C. Atkinson, and G.S. Loquvam, *Perirenal (Gerota's) fascitis.* The Journal of urology, 1959. **81**(1): p. 76-95.
37. Ravelli, A.C., et al., *Obesity at the age of 50 y in men and women exposed to famine prenatally.* Am J Clin Nutr, 1999. **70**(5): p. 811-816.
38. Patro, R., et al., *Salmon provides fast and bias-aware quantification of transcript expression.* Nature methods, 2017. **14**(4): p. 417-419.
39. Baltimore, D., et al., *A prudent path forward for genomic engineering and germline gene modification.* Science, 2015. **348**(6230): p. 36-38.
40. Rosen, E.D., et al., *Transcriptional regulation of adipogenesis.* Genes & development, 2000. **14**(11): p. 1293-1307.
41. Fathzadeh, M., et al., *FAM13A affects body fat distribution and adipocyte function.* Nat Commun, 2020. **11**(1): p. 1465.
42. Vasanthakumar, A., et al., *Sex-specific adipose tissue imprinting of regulatory T cells.* Nature, 2020. **579**(7800): p. 581-585.
43. Stephenson, E.J., et al., *Chronic high dietary sucrose induces sexually dimorphic metabolic adaptations in liver and adipose tissue.* bioRxiv, 2020: p. 2020.05.20.106922.
44. Rey, F., et al., *Transcriptome Analysis of Subcutaneous Adipose Tissue from Severely Obese Patients Highlights Deregulation Profiles in Coding and Non-Coding Oncogenes.* Int J Mol Sci, 2021. **22**(4).
45. Norheim, F., et al., *Gene-by-Sex Interactions in Mitochondrial Functions and Cardio-Metabolic Traits.* Cell Metab, 2019. **29**(4): p. 932-949.e4.
46. Ma, S., et al., *Caloric Restriction Reprograms the Single-Cell Transcriptional Landscape of Rattus Norvegicus Aging.* Cell, 2020. **180**(5): p. 984-1001.e22.

47. Hahn, O., et al., *A nutritional memory effect counteracts benefits of dietary restriction in old mice.* Nat Metab, 2019. **1**(11): p. 1059-1073.
48. Team, R., *RStudio: Integrated Development Environment for R.* 2020.
49. Zhou, G., et al., *NetworkAnalyst 3.0: a visual analytics platform for comprehensive gene expression profiling and meta-analysis.* Nucleic Acids Research, 2019. **47**(W1): p. W234-W241.
50. Bailey, T.L., et al., *MEME Suite: tools for motif discovery and searching.* Nucleic Acids Research, 2009. **37**(suppl_2): p. W202-W208.
51. Shelton, E., et al., *Transcriptional profiling reveals ductus arteriosus-specific genes that regulate vascular tone.* Physiol Genomics, 2014. **46**(13): p. 457-66.
52. Camacho, L.E., et al., *Enhanced insulin secretion and insulin sensitivity in young lambs with placental insufficiency-induced intrauterine growth restriction.* Am J Physiol Regul Integr Comp Physiol, 2017. **313**(2): p. R101-R109.
53. Swanson, A.M. and A.L. David, *Animal models of fetal growth restriction: Considerations for translational medicine.* Placenta, 2015. **36**(6): p. 623-30.
54. Desai, M. and M.G. Ross, *Fetal programming of adipose tissue: effects of intrauterine growth restriction and maternal obesity/high-fat diet.* Semin Reprod Med, 2011. **29**(3): p. 237-45.
55. Zimmermann, R., et al., *Fat mobilization in adipose tissue is promoted by adipose triglyceride lipase.* Science, 2004. **306**(5700): p. 1383-1386.
56. Sarr, O., K. Yang, and T.R.H. Regnault, *<i>In Utero</i> Programming of Later Adiposity: The Role of Fetal Growth Restriction.* Journal of Pregnancy, 2012. **2012**: p. 134758.
57. Morrison, J.L., et al., *Fetal growth restriction, catch-up growth and the early origins of insulin resistance and visceral obesity.* Pediatric Nephrology, 2010. **25**(4): p. 669-677.
58. Karastergiou, K., et al., *Sex differences in human adipose tissues - the biology of pear shape.* Biology of sex differences, 2012. **3**(1): p. 13-13.
59. Kautzky-Willer, A., J. Harreiter, and G. Pacini, *Sex and Gender Differences in Risk, Pathophysiology and Complications of Type 2 Diabetes Mellitus.* Endocrine Reviews, 2016. **37**(3): p. 278-316.
60. Arner, P., *Differences in Lipolysis between Human Subcutaneous and Omental Adipose Tissues.* Annals of Medicine, 1995. **27**(4): p. 435-438.
61. Frias, J.P., et al., *Decreased Susceptibility to Fatty Acid–Induced Peripheral Tissue Insulin Resistance in Women.* Diabetes, 2001. **50**(6): p. 1344-1350.
62. Shulman, G.I., *Ectopic fat in insulin resistance, dyslipidemia, and cardiometabolic disease.* N Engl J Med, 2014. **371**(23): p. 2237-8.
63. Eramo, M.J., et al., *The 'mitochondrial contact site and cristae organising system' (MICOS) in health and human disease.* J Biochem, 2020. **167**(3): p. 243-255.
64. Alston, C.L., et al., *A recurrent mitochondrial p. Trp22Arg NDUFB3 variant causes a distinctive facial appearance, short stature and a mild biochemical and clinical phenotype.* Journal of medical genetics, 2016. **53**(9): p. 634-641.
65. Dottino, J.A., et al., *Endometrial biomarkers in premenopausal women with obesity: an at-risk cohort.* American Journal of Obstetrics and Gynecology, 2021. **224**(3): p. 278.e1-278.e14.
66. Huang, X., et al., *The PI3K/AKT pathway in obesity and type 2 diabetes.* International journal of biological sciences, 2018. **14**(11): p. 1483-1496.
67. Goyal, R., et al., *Antenatal maternal hypoxic stress: adaptations of the placental renin-angiotensin system in the mouse.* Placenta, 2011. **32**(2): p. 134-139.
68. Xu, B., et al., *Multiple roles for the non-coding RNA SRA in regulation of adipogenesis and insulin sensitivity.* PLoS One, 2010. **5**(12): p. e14199.
69. Ornoy, A., et al., *Gender dependent effects of testosterone and 17β-estradiol on bone growth and modelling in young mice.* Bone and Mineral, 1994. **24**(1): p. 43-58.

70. Heine, P.A., et al., *Increased adipose tissue in male and female estrogen receptor-α knockout mice.* Proceedings of the National Academy of Sciences, 2000. **97**(23): p. 12729-12734.
71. Wang, Y., et al., *Administration of 17β-estradiol to ovariectomized obese female mice reverses obesity-hypertension through an ACE2-dependent mechanism.* American Journal of Physiology-Endocrinology and Metabolism, 2015. **308**(12): p. E1066-E1075.
72. Fan, W., et al., *Androgen Receptor Null Male Mice Develop Late-Onset Obesity Caused by Decreased Energy Expenditure and Lipolytic Activity but Show Normal Insulin Sensitivity With High Adiponectin Secretion.* Diabetes, 2005. **54**(4): p. 1000-1008.
73. González-García, I., M. Tena-Sempere, and M. López, *Estradiol Regulation of Brown Adipose Tissue Thermogenesis*, in *Sex and Gender Factors Affecting Metabolic Homeostasis, Diabetes and Obesity*, F. Mauvais-Jarvis, Editor. 2017, Springer International Publishing: Cham. p. 315-335.
74. Chang, E., M. Varghese, and K. Singer, *Gender and Sex Differences in Adipose Tissue.* Current Diabetes Reports, 2018. **18**(9): p. 69.
75. Weisberg, S.P., et al., *Obesity is associated with macrophage accumulation in adipose tissue.* The Journal of Clinical Investigation, 2003. **112**(12): p. 1796-1808.
76. Hamdy O, P.S., Al-Ozairi E., *Metabolic Obesity: The Paradox Between Visceral and Subcutaneous Fat.* Current Diabetes Reviews, 2006. **2**(4): p. 367-373.
77. Kim, S.-N., et al., *Sex differences in sympathetic innervation and browning of white adipose tissue of mice.* Biology of Sex Differences, 2016. **7**(1): p. 67.
78. Blaak, E., *Gender differences in fat metabolism.* Curr Opin Clin Nutr Metab Care, 2001. **4**(6): p. 499-502.
79. Ebert, Margaret S. and Phillip A. Sharp, *Roles for MicroRNAs in Conferring Robustness to Biological Processes.* Cell, 2012. **149**(3): p. 515-524.
80. Dai, R. and S.A. Ahmed, *Sexual dimorphism of miRNA expression: a new perspective in understanding the sex bias of autoimmune diseases.* Ther Clin Risk Manag, 2014. **10**: p. 151-63.
81. Yang, F., et al., *Global survey of escape from X inactivation by RNA-sequencing in mouse.* Genome Res, 2010. **20**(5): p. 614-22.
82. Pinheiro, I., L. Dejager, and C. Libert, *X-chromosome-located microRNAs in immunity: might they explain male/female differences? The X chromosome-genomic context may affect X-located miRNAs and downstream signaling, thereby contributing to the enhanced immune response of females.* Bioessays, 2011. **33**(11): p. 791-802.
83. Victoria, B., Y.O. Nunez Lopez, and M.M. Masternak, *MicroRNAs and the metabolic hallmarks of aging.* Mol Cell Endocrinol, 2017. **455**: p. 131-147.
84. Xie, H., B. Lim, and H.F. Lodish, *MicroRNAs Induced During Adipogenesis that Accelerate Fat Cell Development Are Downregulated in Obesity.* Diabetes, 2009. **58**(5): p. 1050-1057.
85. Thomou, T., et al., *Adipose-derived circulating miRNAs regulate gene expression in other tissues.* Nature, 2017. **542**(7642): p. 450-455.
86. Group, R.E.A.S.P.C.W., *Revised 2003 consensus on diagnostic criteria and long-term health risks related to polycystic ovary syndrome (PCOS).* Human reproduction, 2004. **19**(1): p. 41-47.
87. Goyal, R., et al., *Maternal low protein diet: Developmental origin of adult hypertension.* The FASEB Journal, 2009. **23**: p. 776.6-776.6.
88. Zhang, J., et al., *Haploinsufficiency of the E3 ubiquitin-protein ligase gene TRIP12 causes intellectual disability with or without autism spectrum disorders, speech delay, and dysmorphic features.* Human genetics, 2017. **136**(4): p. 377-386.
89. Calderon-Dominguez, M., et al., *Fatty acid metabolism and the basis of brown adipose tissue function.* Adipocyte, 2015. **5**(2): p. 98-118.

90. Behl, T., et al., *Exploring the Genetic Conception of Obesity via the Dual Role of FoxO.* International journal of molecular sciences, 2021. **22**(6): p. 3179.
91. Lizcano, F. and G. Guzmán, *Estrogen Deficiency and the Origin of Obesity during Menopause.* BioMed research international, 2014. **2014**: p. 757461-757461.
92. Ramkumar, P., et al., *JNK-associated Leucine Zipper Protein Functions as a Docking Platform for Polo-like Kinase 1 and Regulation of the Associating Transcription Factor Forkhead Box Protein K1*.* Journal of Biological Chemistry, 2015. **290**(49): p. 29617-29628.
93. Johnson, J.S., et al., *Evaluation of 16S rRNA gene sequencing for species and strain-level microbiome analysis.* Nature Communications, 2019. **10**(1): p. 5029.
94. Bruce, A.W., et al., *Genome-wide analysis of repressor element 1 silencing transcription factor/neuron-restrictive silencing factor (REST/NRSF) target genes.* Proceedings of the National Academy of Sciences of the United States of America, 2004. **101**(28): p. 10458-10463.
95. De Blasio, M.J., et al., *Placental restriction of fetal growth reduces size at birth and alters postnatal growth, feeding activity, and adiposity in the young lamb.* Am J Physiol Regul Integr Comp Physiol, 2007. **292**(2): p. R875-86.
96. Wang, Y., et al., *METTL3 is essential for postnatal development of brown adipose tissue and energy expenditure in mice.* Nature Communications, 2020. **11**(1): p. 1648.
97. Yang, H., et al., *On-Tissue Derivatization of Lipopolysaccharide for Detection of Lipid A Using MALDI-MSI.* Anal Chem, 2020. **92**(20): p. 13667-13671.
98. Ismail, N.A., et al., *Fetuin-A levels in obesity: differences in relation to metabolic syndrome and correlation with clinical and laboratory variables.* Archives of medical science : AMS, 2012. **8**(5): p. 826-833.
99. Moreno-Indias, I., et al., *Adipose tissue infiltration in normal-weight subjects and its impact on metabolic function.* Translational Research, 2016. **172**: p. 6-17.e3.
100. Park, A., W.K. Kim, and K.H. Bae, *Distinction of white, beige and brown adipocytes derived from mesenchymal stem cells.* World J Stem Cells, 2014. **6**(1): p. 33-42.
101. Weir, G., et al., *Substantial Metabolic Activity of Human Brown Adipose Tissue during Warm Conditions and Cold-Induced Lipolysis of Local Triglycerides.* Cell Metabolism, 2018. **27**(6): p. 1348-1355.e4.
102. Svensson, P.-A., et al., *Characterization of brown adipose tissue in the human perirenal depot.* Obesity, 2014. **22**(8): p. 1830-1837.
103. Li, G., et al., *Metabolic adaptation to intermittent fasting is independent of peroxisome proliferator-activated receptor alpha.* Mol Metab, 2018. **7**: p. 80-89.
104. Crume, T.L., et al., *The long-term impact of intrauterine growth restriction in a diverse U.S. cohort of children: the EPOCH study.* Obesity (Silver Spring), 2014. **22**(2): p. 608-15.
105. Ntambi, J.M. and K. Young-Cheul, *Adipocyte Differentiation and Gene Expression.* The Journal of Nutrition, 2000. **130**(12): p. 3122S-3126S.